Please cite this paper as: ***Buscemi, A., Beccali, M., Guarino, S., & Lo Brano, V. (2023). Coupling a road solar thermal collector and borehole thermal energy storage for building heating: First experimental and numerical results. Energy Conversion and Management, 291, 117279.***

Coupling a road solar thermal collector and borehole thermal energy storage for building heating: first experimental and numerical results

Alessandro Buscemi*, Marco Beccali, Stefania Guarino, Lo Brano Valerio

Department of Engineering
University of Palermo, Viale delle Scienze, Palermo, Italy
*Corresponding author e–mail: alessandro.buscemi@unipa.it

Abstract

The adoption of more efficient technologies that integrate renewable resources for heating buildings is a key action for increasing sustainability in the residential sector in the European Union. Borehole thermal energy storage and road thermal collector systems, which have mainly been integrated in colder countries to develop renewable systems aimed at preventing the freezing of road surfaces in winter, could also be used in warmer countries to develop sustainable heating systems for buildings. In this experimental-numerical study, the possibility of integrating these two systems for the heating of buildings located in the Mediterranean region is investigated for the first time. To this end, a pilot plant was built at the facility test site of the University of Palermo, with the aim of demonstrating the possibility of storing solar energy in summer and recovering it in winter. A new methodology is proposed to characterize both the thermal conductivity and diffusivity of the different materials in the design phase of the plant. The results of simulations conducted with a validated numerical model show that the proposed system, characterized by an average annual collector efficiency of 10% and a seasonal storage efficiency of 80%, can reduce the length of borehole heat exchangers by about three times compared with a conventional geothermal heat pump plant.

Keywords

renewable building heating systems, borehole thermal energy storage, road thermal collector, thermal measurements in soils, pilot plants, dynamic numerical simulations.

Please cite this paper as: ***Buscemi, A., Beccali, M., Guarino, S., & Lo Brano, V. (2023). Coupling a road solar thermal collector and borehole thermal energy storage for building heating: First experimental and numerical results. Energy Conversion and Management, 291, 117279.***

Introduction

In 2019, the residential and tertiary sectors accounted for approximately 36.6 % of the total final energy consumption in the European Union (EU) [1]. Most of these energy demands were met by the consumption of fossil fuels resulting in the emission of massive amounts of greenhouse gases. The adoption of more energy-efficient technologies and the integration of renewable resources are key actions for increasing the sustainability of the building sector in the EU [2]. To this end, Seasonal Thermal Energy Storage (STES) systems can contribute significantly to increasing the annual efficiency of sustainable energy-based heating systems [3] by reducing the mismatch between the period when thermal energy is produced (summer) and the period when this energy is supplied to end users (winter) [4]. Among STESs, Borehole Thermal Energy Storage (BTES) systems, in which soil is used as a medium for sensible heat storage, are beginning to represent a possible economic alternative to large cogeneration plants with the aim of reducing the greenhouse gas emissions of district heating systems [5]. For this purpose, both the possibility of integrating BTES with different types of solar collectors [6] and adapting these systems to various energy sources, such as industrial waste heat and that generated by Combined Heat and Power (CHP) systems, has been recently studied [7]. More generally, there is a growing interest in BTES systems as evidenced by some studies of their possible applications found in the literature, including: the thermodynamic assessment of a large BTES integrated in the Heating Ventilating and Air Conditioning (HVAC) system of a university campus building in Canada [8]; the techno-economic analysis of a BTES charged with the heat from a CHP plant and aimed at heating a building on a university campus in the state of New York (NYS) [9]; the comparative analysis between a solar-powered BTES plant and a sewage heat recovery system to replace a natural gas boiler in two residential buildings with 826 apartment units in Canada [10]; two studies of solar-powered BTES systems for heating a school building in southern Italy [11] and for heating and producing domestic hot water for a 10,000 m^2 multi-apartment building located near Paris, France [12]; and the analysis of a large-scale industrial waste heat heating system, located in China that integrates a BTES system and an absorption heat pump [13].

Among the latest solar technologies that could be profitably integrated with BTES systems are Road Thermal Collector (RTC) systems that can harvest solar energy from the surface layers of the asphalt used to build car parks or roads [14]. The thermal capacity of asphalt mixtures and their high absorption of solar radiation are, in fact, the reasons for determining the high surface

temperature of RTC systems in summer, and thus, their potential as systems to collect a great amount of solar energy [15]. A review of large-scale RTC projects [16] shows that most of these systems are used to prevent snow and ice accumulation on road surfaces, although their extensive use could also be useful in reducing air temperatures in urban areas [17] contributing to the possible mitigation of the heat island effect [18].

In recent years, several numerical models capable of simulating the operation of BTES systems have been proposed and used to perform sensitivity analyses, including: a new method (called Multi Degree of Freedom) by which the influence of thermal conductivity of rock masses was analyzed [19]; a model in FEFLOW 6.1. 2 was used to study different borehole heat exchanger (BHE) arrangements also considering varying values of the thermal and hydraulic properties of the soils [20]; two Finite Element Method (FEM)-based models, developed on ANSYS, to evaluate the influence of borehole slope [21] and heat transfer fluid inlet temperature [22]; and, more recently, a MATLAB model used to test the impact of 10 different design parameters, including flow rate and heat transfer fluid temperature [23].

Despite the development of these sophisticated numerical models, a recent numerical-experimental work [24] demonstrated how the incorrect determination of both the thermal conductivity and volumetric heat capacity values of the soil can introduce significant uncertainties in the design and operation of BTES systems. By way of example, in the case of one of the largest Sweden BTES systems, located at Xylem's production plant in Emmaboda, the average thermal conductivity values of the soil obtained from Thermal Response Tests (TRT) conducted on pilot BHE prior to the construction of the final system provided much lower values than those that could be evaluated from the monitoring data of the first 7 years of operation of the same system [25]. For this same case, the results of numerical simulations carried out on a BTES model developed in the IDA ICE 4.8 environment showed differences between calculated and measured BTES temperature values up to a maximum of 15 °C, attributing an incorrect characterization of the soil volumetric heat capacity [26]. In another, more recent numerical study, conducted using a model developed with Modelica libraries, the energy performance of a 0.5 million m^3 BTES integrated into the district heating system in Chifeng, China, was evaluated, obtaining significant deviations between simulated and measured on-site temperatures during the first 7 months of plant operation. [27]. In the same paper, the numerical procedure followed to assess the average values of the thermal conductivity and the volumetric heat capacity of the soil

using result data from three TRTs is described. Operating data measured for 225 days for the same BTES plant in Chifeng, China, were used in a recent work [24] to test a new numerical back-analysis methodology based on the use of a modified version of the Duct Ground Heat Storage Model (DST) [28]. This method made it possible to estimate the values of thermal conductivity and volumetric heat capacity of the different soil layers, which, taken as model parameters, allow a more realistic simulation of the temperature values measured in the BTES during its operation. This interesting study also showed that the average value of soil thermal conductivity calculated from those of the different soil layers is congruent with that obtained from the TRT results, while the average value of soil volumetric heat capacity calculated in the two different ways is not the same.

Similar to what has been observed for BTES systems, several numerical models have been developed in recent years to evaluate the producibility of RTC systems. These models have been validated using temperature data recorded on pilot RTC plants. Among these approaches we can mention: a new numerical model called HyRoSim that was used to perform the energy assessment of a 70 m^2 pilot RTC built in Östersund, Sweden [29]; a 3D FEM model developed in COMSOL Multiphysics to perform a back analysis of the thermal properties of a 65 m^2 pilot RTC built at Antwerp, Belgium [30] that was subjected to several operational tests [31]; a COMSOL model that was validated with data from a TRT performed on a 42 m^2 pilot RTC built and instrumented in Adelaide, South Australia [32]; and another FEM model developed in COMSOL Multiphysics that was used to perform a back analysis of the thermal conductivity values of the layers of an outdoor asphalt surface in Vaasa, Finland, using temperature data measured at different depths [33]. The model was then also used to simulate the operation of an RTC at the same site.

An analysis of the most recent literature that has been reviewed briefly above shows that the study of the integration of RTC and BTES systems has been directed mainly to the optimization of systems capable of preventing the formation of ice on road surfaces especially in climatic zones characterized by cold winters (there are no examples of this type of system implemented in the Mediterranean). In addition, the most efficient methods suggested for characterizing the soil thermal properties of BTES systems and the materials comprising the RTCs are based on the numerical back analysis of temperature data recorded during the monitoring of already built plants and are, from this point of view, of little use in the design phase of these systems.

Please cite this paper as: ***Buscemi, A., Beccali, M., Guarino, S., & Lo Brano, V. (2023). Coupling a road solar thermal collector and borehole thermal energy storage for building heating: First experimental and numerical results. Energy Conversion and Management, 291, 117279.***

In this research work, for the first time, the possibility of integrating an RTC and a BTES with the aim of heating a non-residential building located in the Mediterranean is analysed. To this end a new pilot plant integrating a 200 m^2 RTC and a BTES consisting of 24 boreholes 15 m long was built in a car park on the university campus as part of a new project at the University of Palermo (Italy) entitled "Sustainable Model and Renewable Thinking Energy Parking" (SMARTEP) [12]. This experimental plant will demonstrate that it is possible to store in the BTES the solar thermal energy produced by the RTC in the summer period and to recover it in the winter period through a dry-cooler emulating the evaporator of a heat pump. The aim of the work is also to propose and experimentally validate a new approach aimed at characterizing the thermophysical properties (thermal conductivity and volumetric heat capacity) of the different soil layers of the BHE and those of the RTC at the design stage. The proposed methodology, (which is described in the methods section in more detail) is based on the construction of a pilot BHE and a small-scale prototype of the RTC, both instrumented at different depths and can be replicated for the design of larger systems This paper discusses the preliminary results of the *in situ* experimental campaign based on the proposed methodology. Through the results of this experimentation, a numerical model of the plant developed using the software Transient System Simulation Tool (TRNSYS) was calibrated. Hourly-based dynamic simulations of the operation of the plant in its first 5 years of life allowed both the sizing of the BTES in terms of the total number and distance of BHEs, and the definition of the annual energy that can be recovered in the winter period to be delivered to the evaporators of a heat pump. A comparison with a conventional Geothermal Heat Pump (GHP) [34] shows that the proposed RTC-BTES system makes it possible to reduce the overall length of the exchangers by about three times.

Materials and methods

Optimization of BTES systems requires in-situ experimentation and the use of numerical models for dynamic simulations of the operating conditions. In this section, the methods adopted in this study for this purpose are briefly described.

2.1 Schematic description of the studied plant

As outlined in the introduction, a design criterion for a building heating system integrating an RTC, a BTES, and a heat pump is proposed in this paper. The RTC systems are, usually, realized through

horizontal exchanger tubes that are embedded in the uppermost layers of a road pavement [35] while the BTES consists of a system of vertical Borehole Thermal Exchangers (BHEs) which are normally arranged at short distances from each other (so as to increase their mutual thermal interference). Referring to the schematic layout shown in Fig. 1, the operation of these kinds of systems can be described as follows: during the summer period, which is characterized by higher solar irradiation, the Heat Transfer Fluid (HTF) circulating between the RTC and BTES (along the closed loop A-B-C-D-E-F-A depicted in Fig.1) allows the heat produced by the solar collector to be transferred to a volume of soil through the system of Borehole Heat Exchangers (BHEs); in the following winter period, the circulation direction of the HTF is reversed (see the closed loop C-B-G-E-D-C in Fig. 1) and the heat stored in the soil is extracted through the BHEs of the BTES and transferred to the heat exchanger of the evaporator of the heat pump, which is used to cover the heating demand of a building.

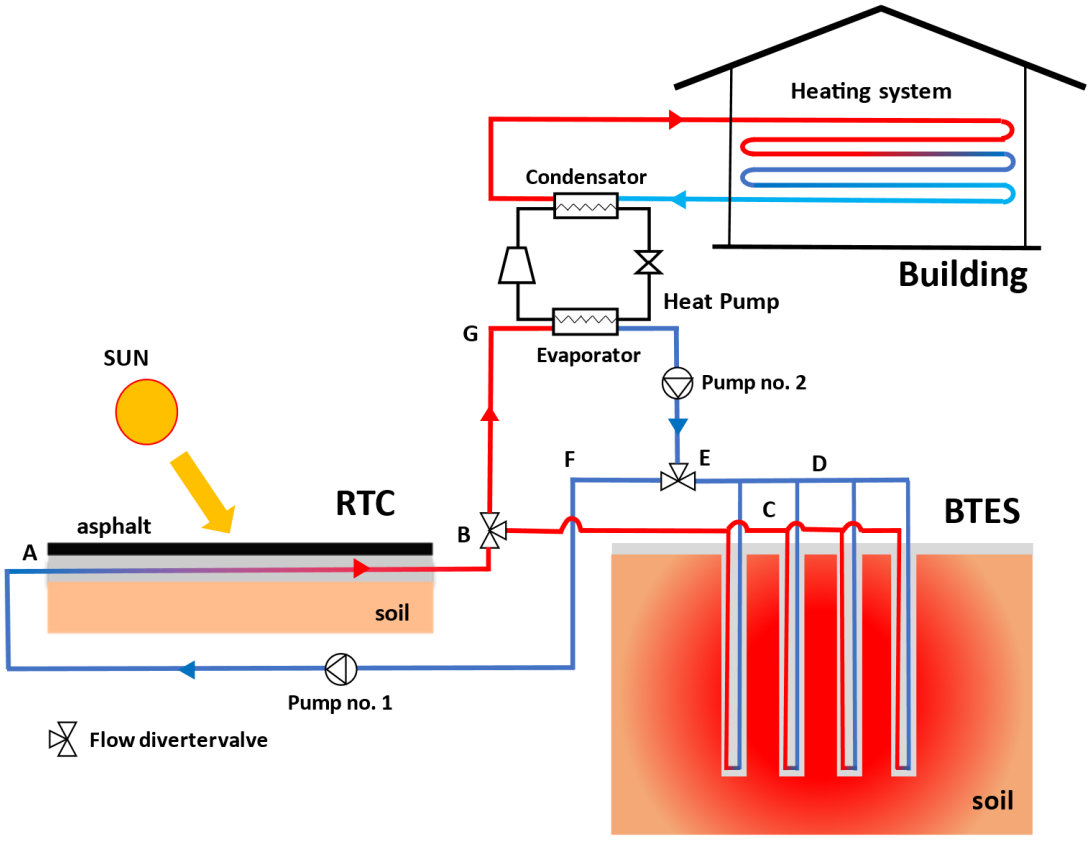

Figure 1. Schematic layout of a building heating system consisting of an RTC, a BTES and a heat pump.

The main function of the BTES is, therefore, to enable the seasonal storage of solar-generated thermal energy by solving the problem of temporal mismatch between the period of highest heating demand of the building (winter) and that of greatest availability of solar radiation (summer). As an example of the operation of this type of plant in the Mediterranean area, a numerical study [11] showed that a system integrating flat-plate solar collectors (instead of RTC), a BTES and a heat pump is able to cover more than 70 % of the winter heating demand of a school with solar energy produced in summer. In the case of the present study, on the other hand, a real-scale pilot system was implemented inside a car park on the Palermo University campus, with the primary objective of demonstrating the actual operating efficiency of this plant scheme over the years through a continuous monitoring system. The studied pilot plant is not connected to a real heating system, but the operation of the heat pump is emulated using a dry-cooler through which the heat extracted from the BTES in the winter period can be rejected into the air. A detailed description of both the stratigraphy of the RTC and the geometry and materials used for the BHEs will be dealt with in the following paragraphs.

2.2 Proposed methodology for the characterization of the material properties

As mentioned in the introduction, this study introduces a new numerical-experimental methodology for thoroughly characterizing the thermophysical properties (thermal conductivity and diffusivity) of the materials used in BTES and RTC during the initial stages of plant design. The following paragraphs provide a detailed explanation of this methodology, which can be summarized as follows:

1. realization of one or more BHE pilots to be instrumented with thermal sensors in the grout at different depths (resistance thermometers or fiber optic temperature sensing system) and a small-scale RTC (even without the presence of exchanger tubes) to be instrumented with thermal sensors at the interface of each layer of material of which it is made;
2. recording, over a sufficient period of time, of the temperature changes at different depths in both the RTC and the pilot BHE related to the interactions of these materials with changes in atmospheric conditions (e.g. variations in air temperature and surface solar radiation). Measurements conducted over an extended period in the BHE pilot, when TRTs are not

being carried out, can be utilized to establish the undisturbed subsurface thermal profile (also determining the yearly average soil temperature), as well as potentially identifying the impact of groundwater flows on variations in deep soil temperature over seasons.

3. execution of a series of TRTs preferably made using heating cables (to exclude from the analyses the effects related to possible uncertainties in the determination of water flow rate in the exchanger tubes). Thermal sensors embedded in the grout will be used to measure temperature values at different depths both during the test execution and in the later stages of soil cooling. Series of TRTs may be repeated several times, and each time the heating cables will be removed and reinstalled so as to ensure replicability of measurements and minimize the possible effect of indeterminacy of cable position on sensor measurements at different depths.
4. TRTs will possibly be temporarily interrupted if it is necessary to make measurements of the water temperature in the BHE pipe through a miniature sensor device [36]. These additional experimental data may be useful in making a comparison between the two different measurement systems;
5. the thermal measurements taken in the RTC during the monitoring period can be used to characterize both the thermal conductivity and the thermal diffusivity of the different layers of materials that make up the collector. For this purpose, it will be sufficient to perform numerical back analyses employing a 1D FEM model describing the stratigraphy of the RTC. In this work, in order to reduce the number of parameters to be determined with this type of analysis, literature values were assumed for the specific heat of the different materials and empirical constitutive relationships were employed that link the thermal conductivity values of asphalt or concrete to those of their density [37,38]. In this way, parametric analyses were conducted by searching for density values of different materials that minimize the error between measured and modeled temperature values;
6. the temperature values measured, at different depths, during the execution of the TRTs can then be modeled using the analytical solution of the infinite line-source problem [39] in order to define the thermal conductivity values of the soil that correspond to each measurement depth. Once the thermal conductivity values have been defined, numerical back analyses can also be performed using a 2D FEM model of the cross section of the BHE and the surrounding soil in order to make an estimate of the thermal diffusivity of the soil at each

measurement depth. With these simulations, the values of the thermophysical properties of the grout can also be estimated;

7. the temperature values recorded in the shallowest part of the pilot BHE (up to about 10 meters below the ground level) during periods when no TRTs were taking place can be used, as will be shown below, to determine an average value of the thermal diffusivity of the soil through the use of an analytical solution. This value can be compared with the one defined by the analyses described in point 2.

2.3 Experimental prospective campaign

More than a year before the pilot plant was built, both a small-scale prototype of the RTC [35] and a pilot BHE were realized in the proximity of the site of interest and they were instrumented with thermal sensors. The experimental data collected during the thermal measurements performed on these prototypes were used to calibrate the numerical models employed to size the BTES.

2.3.1 Instrumented prototype of the road thermal collector and tests

In order to design the RTC, different geometries and construction solutions were analyzed among those proposed in the literature for this kind of collector [35]. The RTC stratigraphy that was finally selected for the construction of the prototype (and later also for the final pilot plant) is depicted in Fig. 2, in which, from top to bottom, the following strata can be identified: the asphalt-binder layer (with a total thickness of 11 cm), the conductive concrete layer (7 cm thick) where the thermal exchanger pipes of the collector were embedded, and the lightened concrete layer (with a thickness of about 50 cm) used as an insulating material between the layer of the pipe and the underlying soil. High-density cross-linked polyethylene (PeX-A) pipes with an outer diameter of D_{po} = 0.032 m and a thickness of 2.9 mm were used as horizontal heat exchangers. The center of each pipe was placed at a depth of 14.5 cm with respect to the surface of the RTC and with a spacing of 25 cm.

Finally, during the construction of one of the small-scale prototypes, five thermal sensors (Pt100 A, B, C and D) were immersed at different depths in the different layers of the RTC (see the red dots in Fig. 2): Sensor A is located inside the asphalt layer at a depth of 3 cm from the top surface; Sensors B, D and E were placed at the interface between the different layers of the RTC; and Sensor C was stuck onto the outer surface of one of the exchanger tubes.

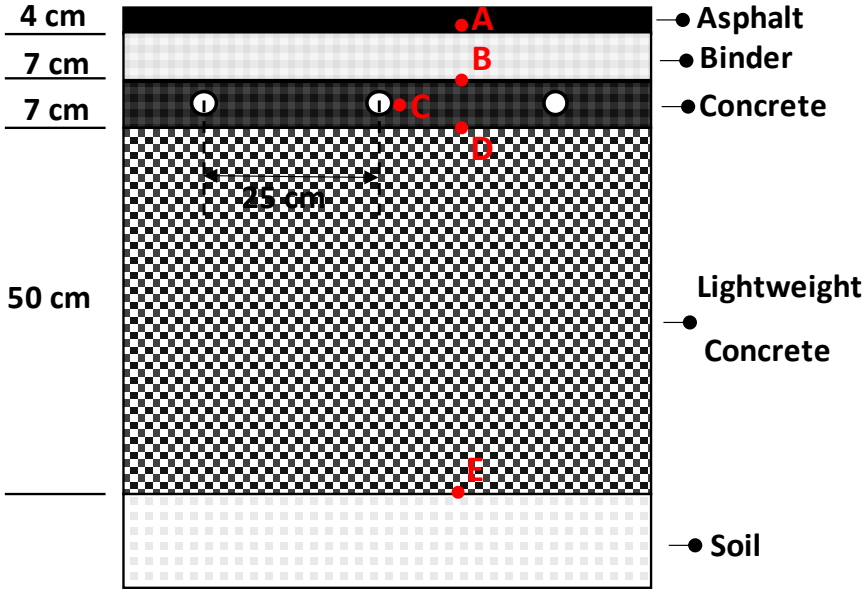

Figure 2. Stratigraphy of the road thermal collector and location of the 5 thermal sensors (Pt100 A, B, C, D and E) in the small-scale prototype.

The sensor system just described for the prototype, which was later replicated in two instrumented sections of the RTC of the final plant, enabled the real-time monitoring of temperature changes over time (every 10'). As will be described in the next section, the experimental data collected in the first 43 days of measurements from the small-scale prototype were used to characterize the thermophysical properties of different materials through the use of numerical models.

2.3.2 Instrumented pilot borehole and tests

The first step in defining the geometry of the BTES was to carry out a geothermal prospective campaign. This *in situ* investigation was employed to: define the different geological structures; obtain soil samples for index testing; provide information on groundwater table position; realize a pilot BHE; install thermal sensors in the borehole; and perform a TRT on the BHE. To this end, a geognostic borehole with a diameter of D_b = 0.14 m and a depth of H_b = 30 m were drilled using a non-destructive technique (see Fig. 3).

Figure 3. Simplified rotary drilling rig and soil sample boxes during the *in situ* soil investigation campaign.

Subsequently, a pilot instrumented BHE was installed inside the existing borehole by: 1) installing a single U-tube (with an external pipe diameter D_{po} = 0.032 m and thickness 2.9 mm); 2) placing 10 thermal sensors (Pt1000) at different depths from the soil surface. The borehole (with U-pipe and sensors) was, finally, sealed with a grout consisting of a mix of bentonite and concrete. Fig. 4.a shows the geometry of the cross-sections of the pilot BHE (characterized by a shank space of x_p = 3.9 cm) in which the approximate position x_{TS} of the generic thermal sensor relative to the center of the borehole is also shown. In turn, Fig. 4.b shows the positions (with their relative depths relative to the surface level) of the thermal sensors that were embedded in the grout of the pilot BHE (Pt1000 A, B, C, D, E, F, G, H, I, and J). The particular arrangement of temperature sensors, denser at the surface and more widely spaced at depth, was chosen to more accurately detail the changes in soil temperature over time, which are greater nearer the surface [40]. These thermal sensors allow continuous monitoring (every 15') of the soil temperature variations along the length of the borehole. More specifically, these sensors are 3-wire PT1000 sensors with stainless steel terminals and silicone-coated cables. They have a measuring range of -50 to 300 °C and an accuracy of 0.1 °C.

Through the use of these thermal measurements, continuously for more than a year, it was possible to identify the undisturbed profile of the Palermo soils down to a depth of 30 m below the ground level. This data, as will be shown later, made it possible to define the thermal diffusivity of the most superficial soil layers in which the BTES was realized.

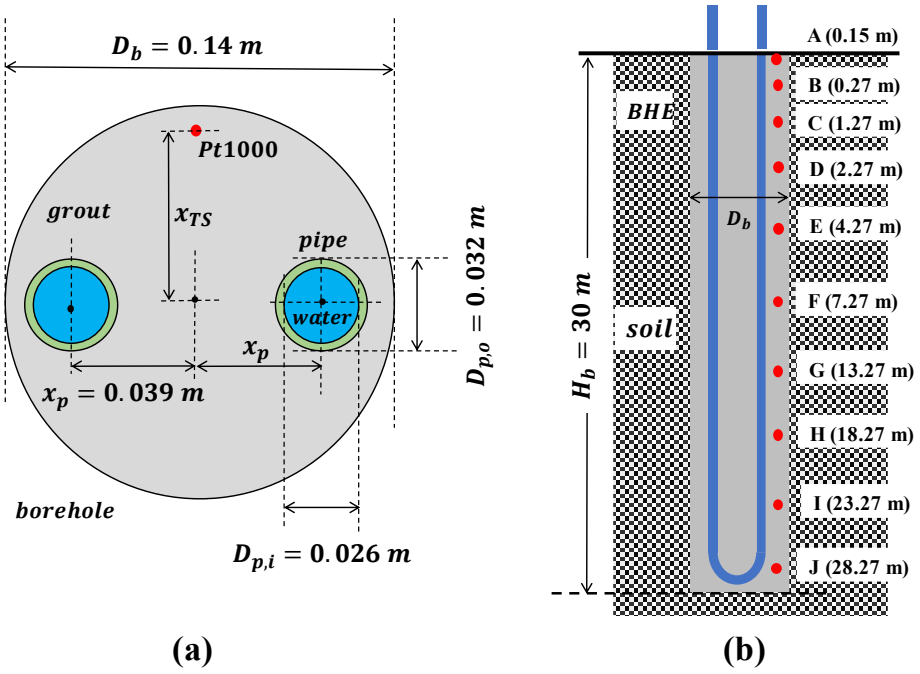

Figure 4. Transversal (a) and longitudinal (b) sections of the single U-tube BHE with the 10 thermal sensor positions (Pt1000 A, B, C, D, E, F, G, H, I and J).

In addition, the ability to monitor grout temperatures along the development of the probe allowed the performance of unconventional TRTs on the pilot BHE:

An initial TRT was performed immediately after the pilot BHE was built. This test, which lasted about 72 h, was carried out by transferring a constant heat flux (of about 1800 W) to the BHE and measuring both changes in grout and water temperatures inside the exchanger tube at different depths along the borehole development. To carry out the test, two heating cables (each capable of transferring 30 W/m) were inserted, one into each of the two legs of the U-tube, and a new type of miniaturized sensor device (GEOsniff® manufactured by Enoware) [36] was used to measure the temperature of the water inside the tubes at the different depths. Measurements of the water column temperature profile were performed periodically (24, 48 and 72 hours after the start of the test, respectively) by temporarily removing the heating cables and inserting the miniaturized sensor device.

The periodic and temporary removals of the heating cables from the BHE tubes caused disturbances to the thermal profile measured by the grout sensors. To overcome this problem, a second set of two TRTs was carried out in which the heating cables were left inside the tubes for the entire duration of the monitoring period and only the evolution in the grout temperatures and no longer that of the water column was recorded. The two TRTs were performed as follows: an initial TRT, performed by imposing a heat output of 60 W/m along the BHE, was carried out by keeping the heating cables on for 12 days. The cables were then kept off for an additional 12 days. At the end of this period, a second TRT, imposing the same thermal power of the first test, was performed by leaving the heating cables on for about 14 hours. The results of all the TRTs allowed, as will be described in the results, the characterization of both the thermal conductivity λ_s and thermal diffusivity α_s of the soil at different depths and those of the materials that constitute the BHE.

2.4 Numerical modeling approach

Both analytical solutions available in the literature and numerical models implemented through the Finite Element Method (FEM) were used for the analysis of all thermal measurements performed on the RTC and the pilot BHE. These techniques enabled the thermo-physical characterization of both the materials used to build the RTC and the soils on which the BTES was subsequently constructed. Finally, a detailed model of the RTC-BTES plant was developed using the TRNSYS framework in order to perform dynamic simulations of the energy performance of the pilot plant during its first 5 years of operation. The types used in TRNSYS were calibrated using the material parameters obtained from the experimental campaign analyses performed on the pilot RTC and BHE.

2.4.1 Analytical solutions

The undisturbed soil temperature measurements recorded for about 480 days (before the pilot plant was built) by 5 of the 10 sensors embedded in the pilot BHE (particularly the Pt1000 A, B, C, D and F in Fig. 4) and were interpreted by means of an appropriate analytical solution of the enthalpy conservation equation with the aim of defining an average value of the thermal diffusivity α_s of the first 7 m of soils. In fact, if the soil domain can be assimilated to an infinitely extended semi-space with uniform thermal conditions on its upper and lower boundaries and the medium is characterized

by being homogeneous and isotropic with respect to thermal diffusivity α_s, it is possible to write the heat conservation equation in one-dimensional form [41] as follows:

$$\frac{dT}{dt} = \alpha_s \cdot \frac{\partial^2 T}{\partial z^2} \tag{1}$$

where T is the soil temperature, t is the time and z is the spatial coordinate along the vertical axis (z is zero on the ground plane and increases positively as depth increases). Under these assumptions, if on the upper boundary the temperature can be modeled with a periodic trend in time, for example through the following sinusoidal relationship:

$$T_{sup}(t) = \overline{T}_{sup} + A_{sup} \cdot \sin\left[\omega \cdot (t - t_0)\right] \tag{2}$$

where $\overline{T}_{sup}$ is the average surface temperature, A_{sup} is the amplitude, ω is the pulse and t_0 is a time-lag constant, and if, in addition, the lower boundary temperature of the half-space ($z = +\infty$) is equal to T_{sup}, then it can be shown that an analytical solution to the problem exists, and the soil temperature variations as a function of z and t can be calculated as:

$$T(z;t) = \overline{T}_{sup} + A_{sup} \cdot e^{-\sqrt{\omega/(2\cdot\alpha_s)}\cdot z} \cdot \sin\left[\omega \cdot (t - t_0) - \sqrt{\omega/(2\cdot\alpha_s)} \cdot z\right]. \tag{3}$$

The analytical solution described by Eq. (3) was employed to characterize the average value of the thermal diffusivity of soils through the following procedure:

1. the series of temperature values measured by the most superficial sensors belonging to the pilot BHE (Pt1000 A, B, C, D and F) were averaged on a daily basis (so as to minimize the effect of cycles of daily thermal variation);
2. the series of daily mean temperatures of the sensor Pt1000 A (z = 0.15 m) was modeled by Eq. (2). To this aim, the pulse was calculated as $\omega = 2 \cdot \pi/\tau$ (where the period was fixed to τ = 365 days) while the remaining parameters of Eq. (2) ($\overline{T}_{sup}$, A_{sup}, and t_0) were calculated by the least-squares method, which was used to minimize the sum (extended to 480 days) of the quadratic differences between modeled and measured daily mean temperatures;
3. Eq. (3) was then used to model the changes over time in the temperatures of the other four sensors (Pt1000 B, C, D and F). For this purpose, the value of z corresponding to the depth of each sensor was set in Eq. (3). Then the least-squares method was applied again in order to find the value of α_s, minimizing the total sum of the quadratic differences between the modeled and measured temperatures for the entire period (480 days) and for all four sensors.

Please cite this paper as: ***Buscemi, A., Beccali, M., Guarino, S., & Lo Brano, V. (2023). Coupling a road solar thermal collector and borehole thermal energy storage for building heating: First experimental and numerical results. Energy Conversion and Management, 291, 117279.***

In order to interpret the different series of TRTs performed on the pilot BHE with the aim of determining the thermal conductivity of the medium, the line-source model was used [39]. This theory is based on the analytical solution of the problem of an infinitely extended linear heat source releasing a constant heat flux q (per unit of source length) into an infinite, homogeneous and isotropic medium. Using the analytical solution in the case of a TRT, it can be shown that, once the steady-state conditions of the heat flow inside the borehole are reached, it is possible to model the variation over time of the average value of the water temperature inside the BHE tubes through a relation of the following type [42]:

$$\overline{T}_w(t) = k \cdot \ln(t) + m_w \tag{4}$$

where k and m_w are two constants. The former constant, in particular, is related both to the heat released per unit of length of borehole q and to the average value of the thermal conductivity of soils λ_s by the following relationship [43]:

$$k = q / \left[4 \cdot \pi \cdot \lambda_s\right]. \tag{5}$$

In practice, given the experimental relationship between mean water temperature $\overline{T}_w(t)$ and time, the value of mean soil conductivity λ_s is derived from Eq. (5). In the present analysis, however, the ability to measure the temperatures of both the water and the grout of the BHE along depth made it possible to estimate the variation of k, and thus that of λ_s, with depth. In other words, the change in grout temperatures measured by thermal sensors can be related to time through a relationship of the type:

$$T_g(z,t) = k(z) \cdot \ln(t) + m_g \tag{6}$$

where z describes the position of the sensor, k is a constant function of z, and m_g is another constant that depends both on the position x_{TS} of the particular thermal sensor in the borehole section (see Fig. 4) and the thermophysical properties of the grout.

In the analyses that are presented below, Eq. (4) was used to interpret the water column measurements in the BHE tubes that were performed periodically during the first TRT. Eq. (6) was, on the other hand, used to analyze the thermal measurements performed on the grout during all TRTs (using data of the Pt1000 C, D, E, F, G and I). In both cases it was possible to define the profiles of soil thermal conductivity with depth using Eq. (5). These profiles were then compared to assess the reliability of the method and to define the average thermal conductivity that was used to calibrate the numerical simulation model.

2.4.2 Finite element models

In order to analyze the data measured by the sensors embedded in the different layers of the small-scale prototype of the RTC, it was assumed, for simplicity, that the thermal conditions can be assimilated into those of one-dimensional heat flow directly along z. This is a reasonable assumption considering both the geometry of the RTC and the uniformity of the thermal conditions at the domain boundaries. Under this assumption, the partial differential equation (PDE) governing the heat conservation problem can be written as:

$$\rho_i \cdot c_{p,i} \cdot \frac{dT}{dt} = \lambda_i \cdot \frac{\partial^2 T}{\partial z^2} \tag{7}$$

where ρ_i, $c_{p,i}$ and λ_i are, respectively, the density, the specific heat and the thermal conductivity of the i^{th} material belonging to the domain [41].

Referring to the above, a one-dimensional FEM model using COMSOL Multiphysics® (a commercial finite element software package [44]) was developed to analyze the experimental result data from the measurement tests performed on the small-scale prototype of the RTC. The geometry of the FEM domain considered for these analyses is depicted in Fig. 5. It can be seen from this image that: 1) the computational domain is bounded by the positions of the Pt100-A and Pt100-E sensors of the RTC; 2) the two layers of asphalt and binder were merged into a single material (sub-domain D1); 3) the layers of conductive and lightweight concrete were defined by the sub-domains D2 and D3, respectively.

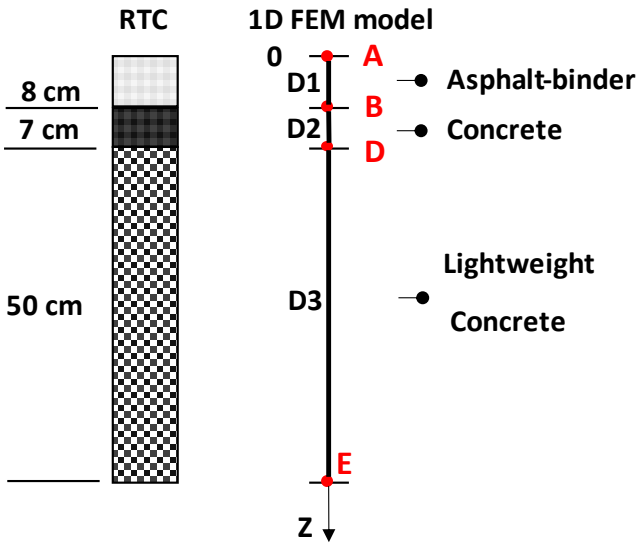

Figure 5. The one-dimensional domain of the RTC prototype FEM model with Pt100 positions (red dot A, B, D and E).

For the characterization of the thermal conductivity of the asphalt-binder material (sub-domain D1), the following empirical expression that relates the thermal conductivity of asphalt-binder λ_a to its density ρ_a was set:

$$\lambda_a = 0.2146 \cdot e^{0.0007 \cdot \rho_a} \quad (8)$$

This expression was defined using experimental data deduced from an experimental study [37] from which, it was also possible to set the specific heat of this material equal to $c_{p,a}$ = 900 J/(kg·K).

The two different concrete strata constituting the remaining part of the RTC differ, essentially, in their density since to prepare the lightweight concrete (sub-domain D3), expanded polystyrene (EPS) particles were added as aggregates to the standard concrete mixture that constitutes the conductive layer (sub-domain D2). The final effect of adding this extremely lightweight thermoplastic, which is characterized by a low value of thermal conductivity close to that of air, is similar to that which would be obtained by increasing the volume of voids in a porous medium [45]. However, a recent review study [38] showed the existence of a general empirical correlation relating the thermal conductivity of concretes λ_c to their densities ρ_c:

$$\lambda_c = 0.0625 \cdot e^{0.0015 \cdot \rho_c} \quad (9)$$

This expression, which was proved to be valid for both low and high-density concretes, was used to characterize the thermal conductivities of both the D2 and the D3 sub-domains of the FEM model adopted for the analyses presented in this study. Finally, the specific heat for both materials was set equal to $c_{p,c}$ = 950 J/(kg·K) considering other experimental results from the literature [46].

To summarize, the thermophysical properties of the three materials comprising the stratigraphy of the RTC were assumed to be functions of their unknown density values. For their definition (and consequently for the thermophysical characterization of these materials) the following steps were taken:

1. A first set of FEM analyses were conducted considering the domain comprised of the sub-domains D1 and D2 (excluding the sub-domain D3). The temperature values measured by Pt100 sensors A and D during the 43-day experimental campaign were imposed as boundary (Dirichlet) conditions on A and D, respectively. Then a series of parametric FEM analyses were conducted iteratively by varying the density values of ρ_a

(in the range 1600-2400 kg/m^3) and those of ρ_c (in the range 2000-2400 kg/m^3) until the combination of densities was found that minimized the error between the temperature values measured by Pt100 C in the RTC and those simulated for the interface C in the FEM model. The error that was minimized through the iterative procedure was defined as the time average of the instantaneous differences, in absolute value, between modeled and measured temperatures.

2. Once the density values for the first two layers (sub-domains D1 and D2) were estimated, a second set of FEM parametric simulations was carried out considering the complete domain. For each simulation, the temperature values measured by the Pt100 sensors A and E during the experimental campaign were imposed at the boundaries A and E of the FEM model domain, respectively. Then, the parametric simulations were conducted iteratively by varying the value of ρ_c for the sub-domains D3 (in the range 500-2200 kg/m^3) until a value of density was found that minimized the error between the temperature values measured by the sensors Pt100 D in the RTC and those simulated for the interface D of the FEM model. The error that was minimized through the iterative procedure was defined in a similar way to step 1.

The procedure described in the previous steps (which made use of experimental measurements and FEM analyses) enabled the complete characterization of the thermophysical properties of the materials constituting the stratigraphy of the RTC which was realized first as a small-scale prototype and then in full-scale as a part of the pilot plant.

A second FEM model of the cross-section of the BHE was developed using COMSOL Multiphysics® with the purpose of simulating the measured variations of the grout temperatures recorded by Pt1000 sensors at the different depths, during the second set of TRTs on the pilot BHE. These simulations aimed to:

- characterize the thermal conductivity of the grout λ_g (and thus the corresponding thermal resistance R_g of the BHE);
- define the position x_{TS} of the thermal sensors within the instrumented borehole sections where they were located after the installation;
- characterize the thermal diffusivity values of soils α_s at different depths.

A description of the two-dimensional FEM model with a triangular mesh used to discretize the calculation domain is depicted in Fig. 6. This domain was set equal to one-quarter of the cross section of the BHE considering that both the geometry and the thermal conditions are symmetric. In the same figure, the following different sub-domains can be identified: water (D1), PeX-A of the U-tube (D2); grout (D3) and soil (D4). For each of these sub-domains the PDE representing the heat conservation equation [47] can be set as:

$$\rho_i \cdot c_{p,i} \cdot \frac{dT}{dt} = \nabla \cdot \left(\lambda_i \cdot \overline{\nabla} T \right) \tag{10}$$

Referring to Fig. 6, the boundary conditions fixed to simulate the TRTs for the different sensor positions are the following:

- Boundary C1: a constant heat flux (Neumann condition) equal to 15 W (corresponding to a global heat flux released from the borehole to the ground during TRT equal to q = 60 W/m);
- Boundary C2: constant temperature (Dirichlet condition) equal to the initial undisturbed soil temperature. This temperature was defined considering the last temperature value recorded by each Pt1000 before the TRTs started.

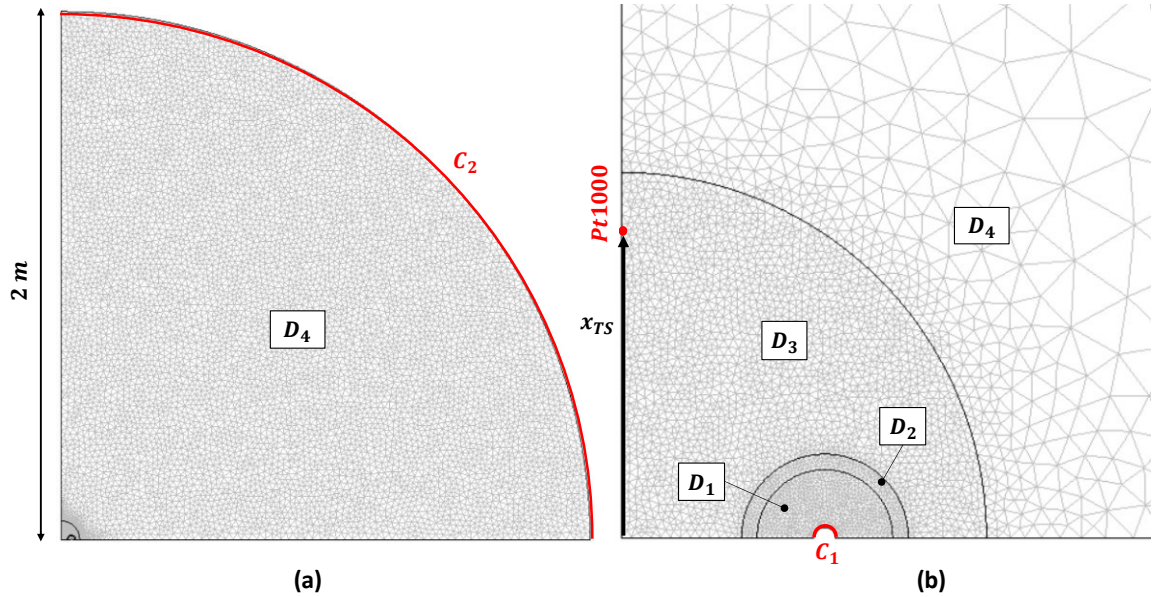

Figure 6. (a) 2D FEM model of a quarter of BHE; (b) detailed view around the borehole.

Regarding the values assumed for some of the thermophysical parameters characterizing Eq. (10) for the sub-domains D1, D2, and D3, reference was made to the data summarized in Table 1.

Concerning sub-domain D4, instead, the soil thermal conductivity values λ_s assumed for the calculations were set considering the results obtained from the elaboration of the TRTs using the line-source method (described above).

Table 1. Thermophysical properties assumed for a BHE.

Sub-domain	Parameter	Units	Value
D1 (water)	density, ρ_w	[kg/m^3]	1000.
D1 (water)	thermal conductivity, λ_w	[W/(m·K)]	0.60
D1 (water)	specific heat, $c_{p,w}$	[J/(kg·K)]	4200
D2 (PeX-A)	density, ρ_p	[kg/m^3]	932
D2 (PeX-A)	thermal conductivity, λ_p	[W/(m·K)]	0.42
D2 (PeX-A)	specific heat, $c_{p,p}$	[J/(kg·K)]	2300
D3 (grout)	volumetric heat capacity, C_g	[J/(m^3·K)]	$3.9 \cdot 10^6$

The remaining parameters (i.e. the soil thermal diffusivity α_s, the values of x_{TS} at different sensor depths and the grout thermal conductivity λ_s) were defined through parametric FEM simulations of the second TRTs performed on the BHE (using the temperature data measured by Pt1000 sensors D, E, F, and G). The procedure followed for these analyses can be summarized as follows:

1. a first-attempt value of the soil thermal diffusivity α_s was set equal to that obtained from the procedure described by Eqs. (1)-(3) using the undisturbed soil temperature data. Then a series of parametric simulations were conducted by iteratively varying x_{TS} and λ_s, in order to find a couple of values minimizing the mean error between the values measured by the Pt1000 G and those calculated by the FEM analyses at the point x_{TS}. For each iteration, the error was calculated as the time average of the instantaneous differences, in absolute value, between the modeled and the measured values of the grout temperature;
2. once the thermal conductivity of the grout was assessed, a second set of parametric numerical simulations were performed considering all the series of data measured by the thermal sensors (Pt1000 D, E, F and G) during the same TRTs. For each of these 5 series, x_{TS} and α_s (in the range of $1 \cdot 10^{-7}$-10^{-6} m^2/s) were iteratively varied until the average error between measured and simulated grout temperatures was minimized.

The calculated values of thermal conductivity and diffusivity of soils were finally processed by a weighted averaging over the thickness of the different soil layers in order to obtain the parameters that were used to calibrate the TRNSYS model of the BTES.

To evaluate the accuracy of the FEM simulation model, both Mean Absolute Error (MAE) and Mean Absolute Percentage Error (MAPE) were calculated. MAE measures the absolute difference between the actual and predicted values and provides an average error value that can be calculated by Eq. (11) [48]:

$$MAE = \frac{1}{N}\sum_{i=0}^{N}|y_i - y| \tag{11}$$

where, N is the total number of samples in the dataset, and y_i and y are the actual value and predicted value of the target variable, respectively. MAPE, on the other hand, measures the percentage difference between the actual and predicted values and provides an average error percentage [49]. The equation for MAPE is as follows:

$$MAPE = \frac{1}{N}\sum_{i=0}^{N}\left|\frac{y_i - y}{y_i}\right| \cdot 100 \tag{12}$$

By calculating both MAE and MAPE, we can get a comprehensive understanding of the accuracy of the regression model in predicting the target variable. MAE and MAPE as error metrics provide different perspectives on the accuracy of the regression method. MAE gives an idea of the average magnitude of the errors, while MAPE expresses the errors as a percentage of the actual values. This allows for a more comprehensive evaluation of the accuracy of the model and can help identify any systematic biases or trends in the predictions.

Finally, the FEM analyses allowed the calculation of the borehole equivalent thermal resistance of the grout R_g which can be modelled as:

$$R_g = \frac{B}{\lambda_g} \tag{13}$$

where B is a dimensionless constant that depends only on the geometry of subdomain D3 [34].

2.4.3 Simulation model of the pilot plant

To dimension the BTES and define the operating conditions of the pilot plant, a numerical model was developed using TRNSYS [50]. Fig. 7 shows the layout integrating the different components of the system under study: RTC, BTES and user. The same figure shows the two different circuits that are activated, through the appropriate use of diverter valves, during the summer and winter months, respectively: a) during the summer charging phase, the hot water leaving the RTC is

delivered to the BTES boreholes from where, after having injected the heat, it returns to the RTC inlet; b) during the winter discharging months, the cold water leaving the user is delivered to the BTES to heat up and then returned to the user. The BTES is usually built in concentric radial zones: the head BHEs are placed in the central part and each of them is connected in series to a corresponding BHE in a more peripheral concentric zone. In this way, heat can be distributed more efficiently in the soil. In addition, to increase storage efficiency, during the charging phase water enters from the central exchangers and exits from the peripheral ones while, during the subsequent discharge phase, the flow is reversed [7]. This technique tends to generate a radial thermocline inside the volume of soil, that is, the central core of the BTES remains warmer and the peripheral zones colder (with an appreciable reduction in the thermal losses from the BTES to the cooler surrounding soil volumes).

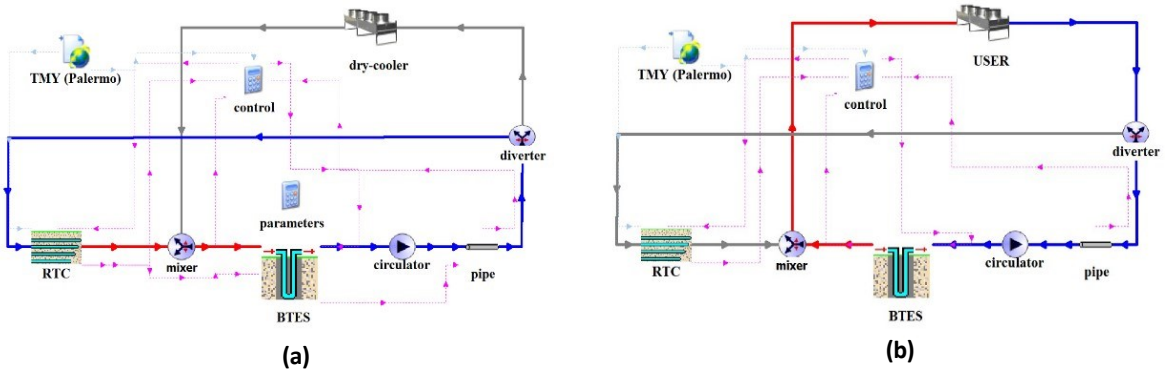

Figure 7. TRNSYS layout of the plant during the charging (a) and discharging (b) phases.

The TRNSYS "Type 997" [50] was used to model the RTC. This type considers a series of parallel horizontal exchangers, filled with flowing water and buried in a volume that may consist of several layers characterized by different material properties [35] (see Fig. 8). For each of the considered layers, the type numerically solves the three-dimensional PDE described by Eq. (10) using the finite difference method. The asphalt temperature T_a, defining the upper boundary condition of the layered volume, is obtained by modeling the energy balance of the asphalt-atmosphere interface [51] as follows:

$$G_h \cdot a_a - h_a \cdot (T_a - T_{air}) - \sigma \cdot \varepsilon_a \cdot (T_a^4 - T_{sky}^4) - \lambda_a \cdot \nabla T_a = 0 \quad (14)$$

where: G_h is the global solar irradiance on a horizontal surface, a_a is the asphalt short-wave radiation absorptivity, h_c is the convective heat transfer coefficient due to the wind, T_{air} is the air temperature, σ is the Stefan–Boltzmann constant and ε_a is the asphalt long-wave radiation emissivity. In the above expression, the gradient of T_a is considered positive if upwards pointing, while the variations of h_a as a function of the wind velocity v_{wind} are modeled using the following empirical expression [52]:

$$h_a = 5.8 + 3.95 \cdot v_{wind} \tag{15}$$

where the second term on the right-hand side disappears for v_{wind} >5 m/s.

Data obtained from the numerical analyses of the experimental data obtained from the temperature measurements on the small-scale RTC were used to calibrate the thermophysical properties of the strata. In addition, for the asphalt layer, a_a = 0.9 and ε_a = 0.9 were assumed [35].

The coupling between the equations which model the enthalpy conservation in the fluid circulating in the exchanger tubes and in the layer containing the exchanger tubes is obtained by introducing the equivalent thermal resistance of the pipes [53], which can be expressed as the sum of a convective and a conductive component as follows:

$$R_p = \frac{\ln\left(D_{po} / D_{pi}\right)}{2 \cdot \pi \cdot \lambda_p} + \frac{1}{\pi \cdot D_{pi} \cdot h_p} \tag{16}$$

where D_{po} and D_{pi} are the outer and inner pipe diameters respectively, λ_p is the pipe thermal conductivity, h_p is the convective heat transfer coefficient within ducts (calculated using the appropriate empirical correlations [54] as a function of the water mass flux rate circulating inside the horizontal exchanger pipes).

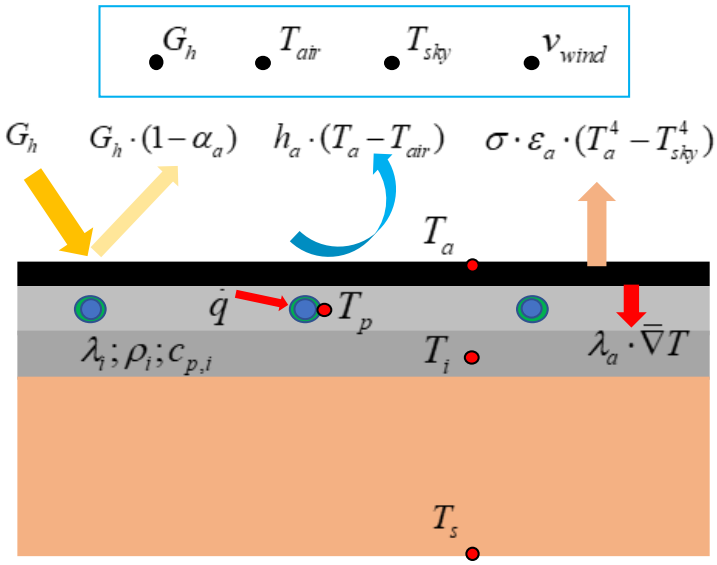

Figure 8. Schematic description of the model implemented by the TRNSYS "Type 997".

To simulate the thermal dynamic response of the BTES the "Type 557" [50] was used. This Type embeds the DST model developed by Hellstrom [28] which requires several input parameters, such as: the total number of boreholes N_b and their depth H_b, their mutual distance d_b, the type of connection between the pipes (series or parallel), the undisturbed soil temperature T_s, the soil thermal conductivity λ_s, the soil heat capacity C_s and the BHE thermal resistance R_b. The layout implemented in the DST model consists of hexagonal solids arranged in a cylindrical symmetrical array where at the centre of each hexagon a BHE is placed [55]. Thus, the conventional volume of the BTES can be calculated using the following expression:

$$V_{BTES} = \pi \cdot N_b \cdot H_b \cdot (0.525 \cdot d_b)^2 \tag{17}$$

"Type 557" has been modified to allow for a variable overall borehole thermal resistance via the following expression [34]:

$$R_b = R_p / 2 + R_g \tag{18}$$

where R_p can be calculated by Eq. (16) and R_g by Eq. (13) as described before. "Type 557" takes into account the possibility of considering an insulating material placed above the top surface of the BTES to reduce the thermal losses to the external environment. To account for this insulation layer in the model, it is necessary to set both its thickness and thermal conductivity.

Finally, for both the above-described TRNSYS models ("Types 997 and 557"):

- the bottom thermal boundary conditions were set equal to the undisturbed soil temperature value characteristic of the studied area;
- the Typical Meteorological Year (TMY) was generated by "Meteonorm" [56] for the plant location in order to define the hourly-based time series of the climatic variables (G_h, T_{air}, T_{sky}, and v_{wind}) needed to perform the numerical simulations.

2.4.4 Comparison with an equivalent conventional geothermal heat pump system

To evaluate the advantage, in terms of overall BHE reduction, of the RTC-BTES system over an equivalent conventional GHP system [34] the following procedure was followed:

1. a new TRNSYS model of a GHP system consisting of a number of BHEs equal to the number of head BHEs of the RTC-BTES system was defined. The distance between the BHEs of the GHP system was, however, set at 8 m (as is usually defined in GHP systems);
2. 5-year dynamic parametric simulations were performed in which the same winter thermal demand profile employed in the RTC-BTES system simulations was imposed and in which the length of the probes was varied;
3. the length of the BHEs was identified at which the average seasonal temperature output from the probes was comparable to that obtained over the same period from the RTC-BTES system simulations.

2.5 Case study

As part of the new project at the University of Palermo (Italy) entitled *Sustainable Model and Renewable Thinking Energy Parking*, an experimental plant, integrating an RTC and a BTES, was set up in a car park on the university campus [35]. The thermal energy produced by the RTC in the summer season will be stored in the BTES and will subsequently be recovered during the winter period to be transferred to a user (which will be emulated using a dry-cooler). Due to the limited availability of space within the car park, the collecting surface area of the RTC was set to approximately 100 m^2. The heat exchanger pipes of the RTC were realized with 16 pipes 20 m long connected in parallel. A detailed stratigraphic section of the RTC was already depicted in Fig. 2. The BTES was built using thermal exchangers with PE-X U-tubes placed in 24 boreholes whose geometrical characteristics are described in Fig. 4.a. Due to space constraints,

it was not possible to occupy a surface area of more than 130 m^2. Thus, the BHEs constituting the BTES were arranged according to an axisymmetric layout, being distributed on three concentric rings (8 per ring) whose radii are respectively: 2.23 m, 4.07 m and 5.28 m. In this way, each BHE insists on a volume of soil that is identical to that of all the others. Each of the 8 BHEs of the central ring was connected in series to one of the 8 BHEs of the second ring, which, in turn, was connected to one of the outermost rings (see Fig. 9).

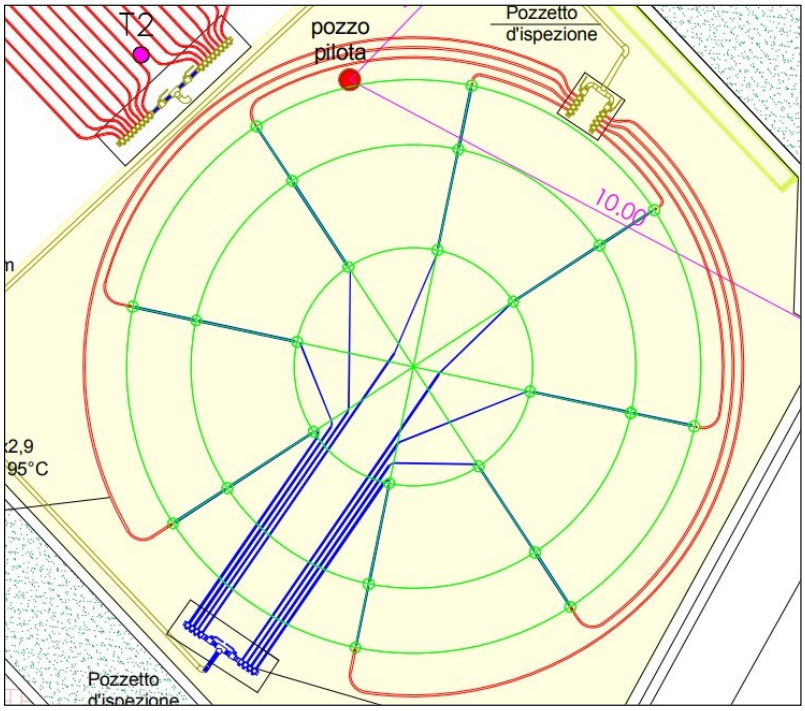

Figure 9. The layout of the 24 BHEs constituting the BTES of the SMARTEP pilot plant.

As previously described, the calculation layout of the DST model requires each borehole to be placed in the centre of a hexagonal solid with an apothem equal to $d_b/2$. Thus the above-described BHEs configurations approximately correspond to a calculation layout in which the BHEs are spaced d_b = 2.5 m apart.

The heads of the BHEs were located at a depth of about 71 cm below the surface of the ground level. This thickness was filled with: a layer of asphalt-binder (11 cm thick); a layer of reinforced concrete (10 cm thick); and a layer of light concrete (50 cm thick). This both provided an insulating layer over the BTES and ensured full operation of the car park.

When the plant starts to operate, it is expected that the BTES charging period will be between April and October. During this period, the mass flow rate circulating between the RTC and the BTES will be set at about $\dot{m}_w$ = 11 m^3/h in order to ensure turbulent flow conditions (with *Re* = 10000) for the fluid circulating in the exchangers of the RTC. These conditions correspond to turbulent flow for the fluid circulating in the tubes of BHEs characterized by *Re* = 20000. During the subsequent winter period (between November and February), the dry-cooler will be turned on daily between 8 a.m. and 7 p.m. to emulate the integration of BTES with the (heat pump) of a building heating system. At this stage, the flow rate of the fluid circulating between the BTES and the dry-cooler will be set equal to $\dot{m}_w$ = 2.5 m^3/h in order to ensure the minimum turbulent flow conditions inside the tubes of the BHEs (*Re* = 2300).

As shown below, the results of the prospective experimental campaign prior to the design phase allowed the maximum length H_b of the BHEs to be defined. In addition, using the calibrated TRNSYS model it was possible to perform a series of parametric simulations of the operation of the pilot plant during its first 5 years of life. These simulations were conducted by varying the thermal jump between the water entering and leaving the dry-cooler with the aim of identifying the maximum annual thermal energy that can be recovered from the BHEs by minimizing the annual changes in the internal energy of the V_{BTES} (i.e. after a complete load and unload cycle). Finally, from the same simulations it was also possible to assess the storage efficiency of the BTES (defined as a ratio of the total discharged energy from the BTES over the total charged energy [11]).

Results and discussion

This section summarizes the most important results of the in situ experimental test campaign carried out both on the RTC prototype and pilot BHE and the results of dynamic simulations of the operation of the full-scale pilot plant during its first 5 years of life.

3.1 Results from the in situ experimental campaign

The soil and rock samples cored from the borehole were ordered according to extraction depth and analyzed. These analyses, together with the geological information already known for the studied area, allowed the reconstruction of a geological cross-section of the soils (see Table 2). Moreover, by inspecting the drilling operation and the water content of the soil samples it was possible to

deduce that the groundwater table is located at a depth of between 25 and 30 m from the ground level.

Table 2. Geological stratigraphy of the plant area.

Lithology	Depth (m)
Sand and gravels	0 – 4.2
Calcarenite (limestone)	4.2 – 12.3
Sandy silts	12.3 -35
Clays	>35

Results from thermal measurements were used, at this preliminary stage, to define the undisturbed thermal profile of the soil down to a depth of 30 m. Fig. 10 shows, as an example, the soil thermal profile measured on 12/01/2021. On that day, an independent measurement of the temperature profile of the water inside the exchanger tubes was obtained using the sensor GEOsniff®.

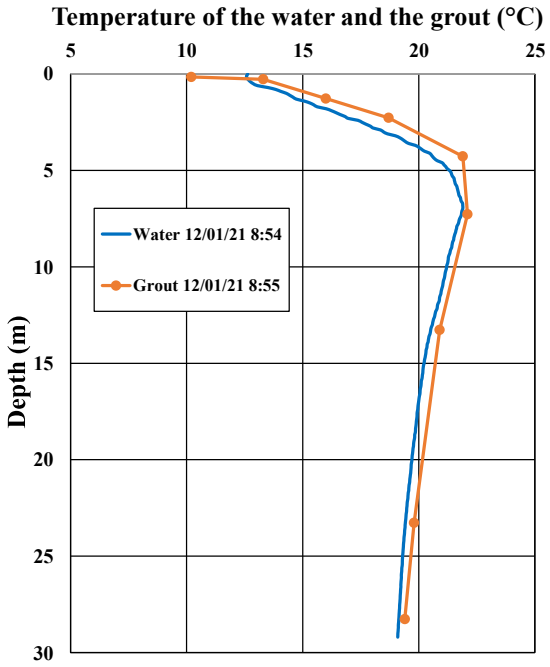

Figure 10. Water and grout temperature profiles measured on 12/01/2021.

The data depicted in Fig. 10 show a good agreement between the temperature values recorded by the two independent measurement systems. The analysis of the obtained undisturbed profile therefore also allowed the assessment of the deep soil temperature value of T_s = 20 °C. This temperature value was imposed as a bottom boundary condition for both the RTC and BTES models.

Moreover, analysing the preliminary results of the experimental campaign described above, it was possible to deduce that: 1) the unsaturated limestone layer shows a higher thermal capacity than the underlying soils; 2) soils with depths of between 2 and 15 m are characterized, in their undisturbed state, by relatively higher temperature values compared to the other layers (this circumstance suggests that radial conduction heat losses from this area of the BTES would be reduced); 3) the convective thermal losses due to the presence of the groundwater table at 25 m below ground level would negatively impact the efficient storage of thermal energy in the soil. These considerations led to setting a maximum design BHE length of H_b = 15 m. Thus, considering that the layout of the BTES consists of 24 BHEs of length H_b=15 m and spaced d_b = 2.5 m, from Eq. (17), it was possible to assume a conventional soil volume of the BTES equal to about V_{BTES} = 1948 m^3.

Once the depth of the BHEs was defined, the soil sample series cored down to this depth (15 m) were analyzed. From these analyses, the following average property values were obtained for these materials: ρ_s = 2700 kg/m^3, c_{ps} = 800 J/(kg·K) and n = 0.3.

3.1.1 Characterization of the soil thermophysical soil properties

Through the measurements made by the Pt1000 sensors of the pilot BHE, it was possible to define the surface temperature variations down to a depth of about 7 m from the ground level. The daily averaged values of these temperatures are shown in Fig. 11 for the Pt1000 A, B, C, D, E and F of the pilot BHE. From the data in the figure, it is possible to notice the heating peaks due to the execution of the first set of TRTs and cooling due to the groundwater flow at the shallowest sensor location.

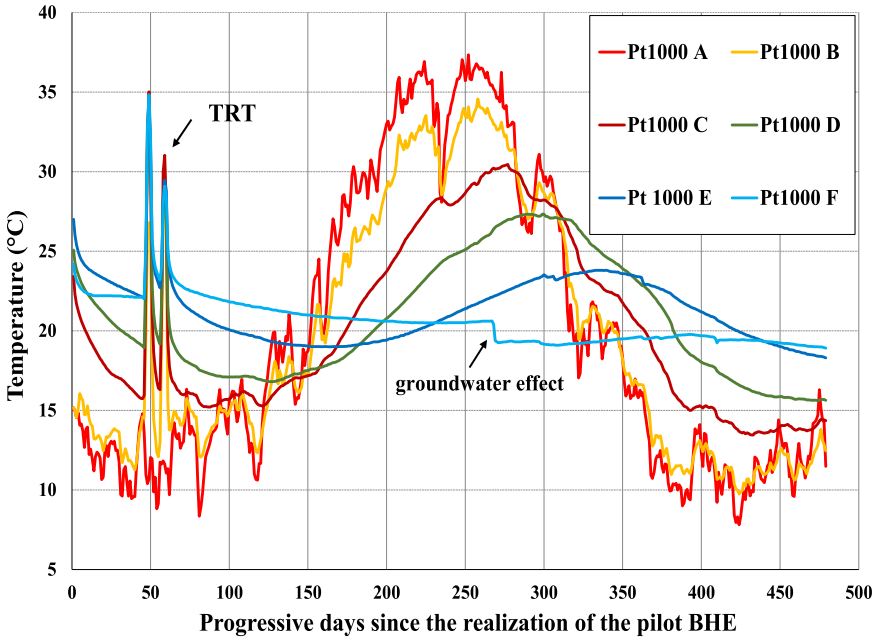

Figure 11. Daily averaged values of the temperatures measured by the Pt1000 sensors.

From the data of Pt1000 A, the following parameters of Eq. (2) were derived: $\overline{T}_{sup}$ = 22.36 °C; A_{sup} = 13.50 °C; t_0 =147.19 day. Thus, by adopting the least-squares method for the fitting of Eq. (3), it was possible to deduce a value of the average thermal diffusivity of soils equal to $\alpha_s = 6.7 \cdot 10^{-7}$ m^2/s. The fluctuations of the soil temperature over time at different depths obtained from the analytical solution described by Eq. (3) are described in Fig. 12.

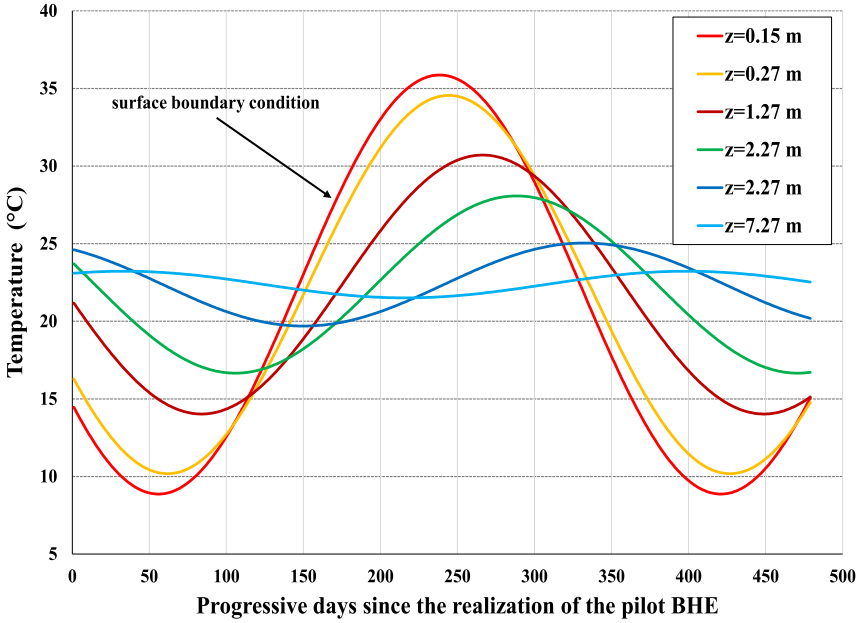

Figure 12. Variations of the soil temperature over time at different depths obtained from the analytical solution described by Eq. (3).

The results of TRTs (series no. 1, 2 and 3) in terms of temperature changes over time for different thermal sensors have been plotted in Fig. 13. These data represent a selection from all those obtained overall during the experimental campaign and refer to those tests whose results showed good replicability. The use of heating cables, although very practical, has the defect of producing localized heat if the cable rests on the inner walls of the BHEs tubes. In addition, the data in Fig. 13 show that the TRTs of the first series are affected by a disturbance due to the extraction of the heating cables during the water column temperature measurements.

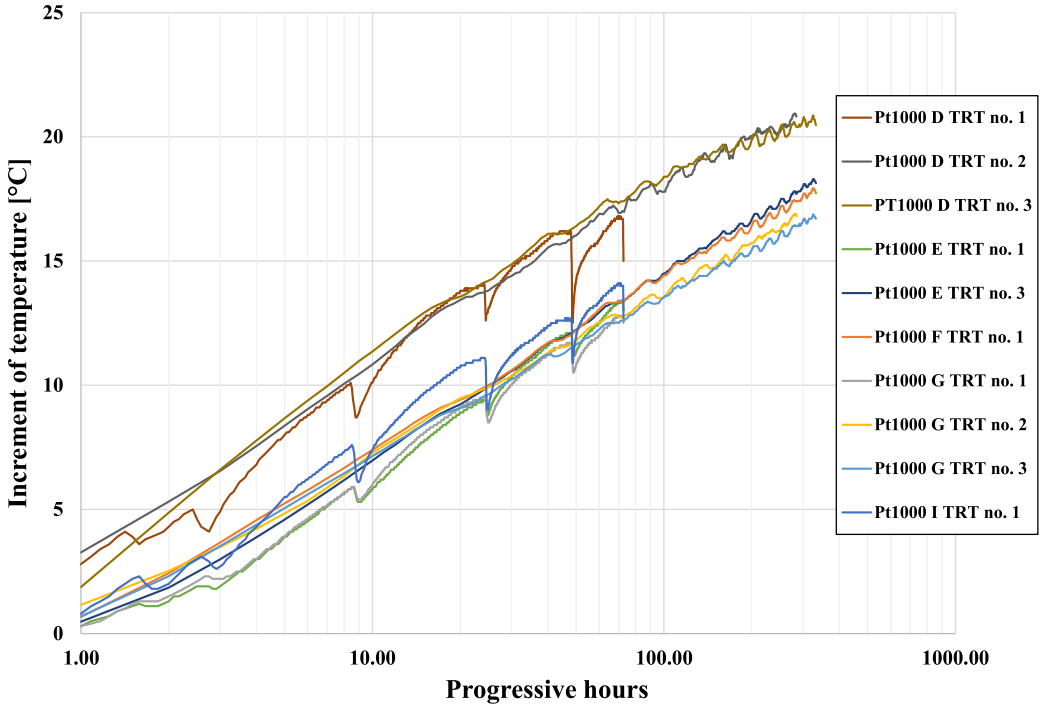

Figure 13. Results of TRTs in terms of temperature changes over time for different thermal sensors.

Processing of the TRT data using the methods described by Eq.s (4)-(6) allowed the definition of the soil thermal conductivity profile with depth. The results of this elaboration are shown in Fig. 14. This figure shows the profiles obtained through water column temperature measurements (TRT series no. 1), and those obtained through the grout temperature measurements (TRT series no. 1, 2 and 3). Data show good agreement with each other and highlight the localized variations in thermal conductivity due to the presence of the limestone blocks. It is also possible to observe an increasing trend in thermal conductivity with depth probably related to the increasing degree of saturation of soils near the location of the water table.

Numerical simulations performed with two-dimensional FEM models were added to the considered analyses. Fig. 15 shows, as an example, a comparison between the temperature changes measured by Pt1000 G during TRTs no. 2 and 3 and the corresponding values obtained from the FEM simulations. The good agreement between measured and modeled values shows that the FEM model can realistically represent the transient thermal response of BHEs. Through FEM modeling it was also possible to define the following parameters for the BHEs: λ_g=1.475 W/(m·K), R_g = 0.074

m·K/W and B = 0.10. In the same figure, the results obtained in terms of MAE using Eq. (11) are reported, which reach a maximum value of 1.43 °C and a total value of 0.19 °C. The MAPE was also calculated on the same dataset using Eq. (12), and a percentage error of 0.6% was obtained.

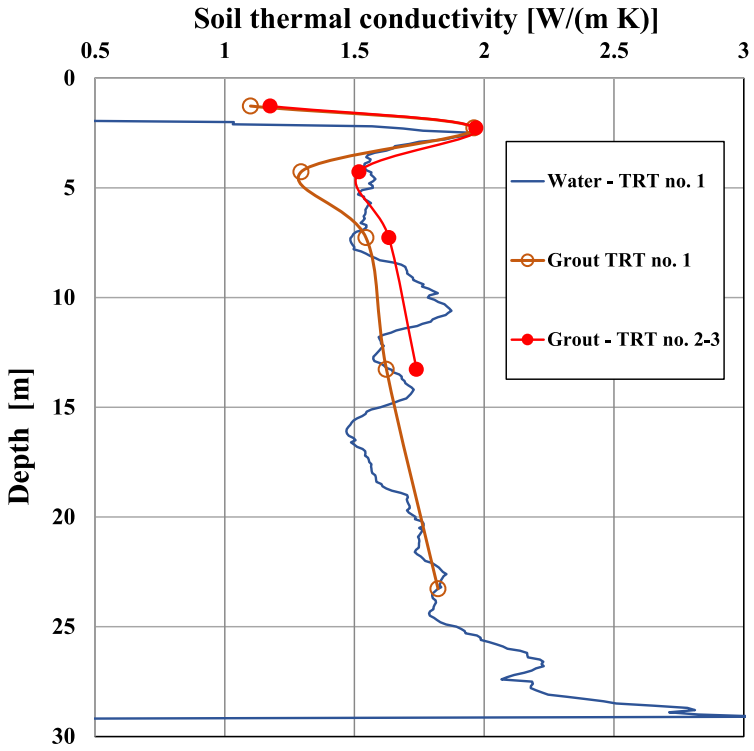

Figure 14. Soil thermal conductivity profiles with depth.

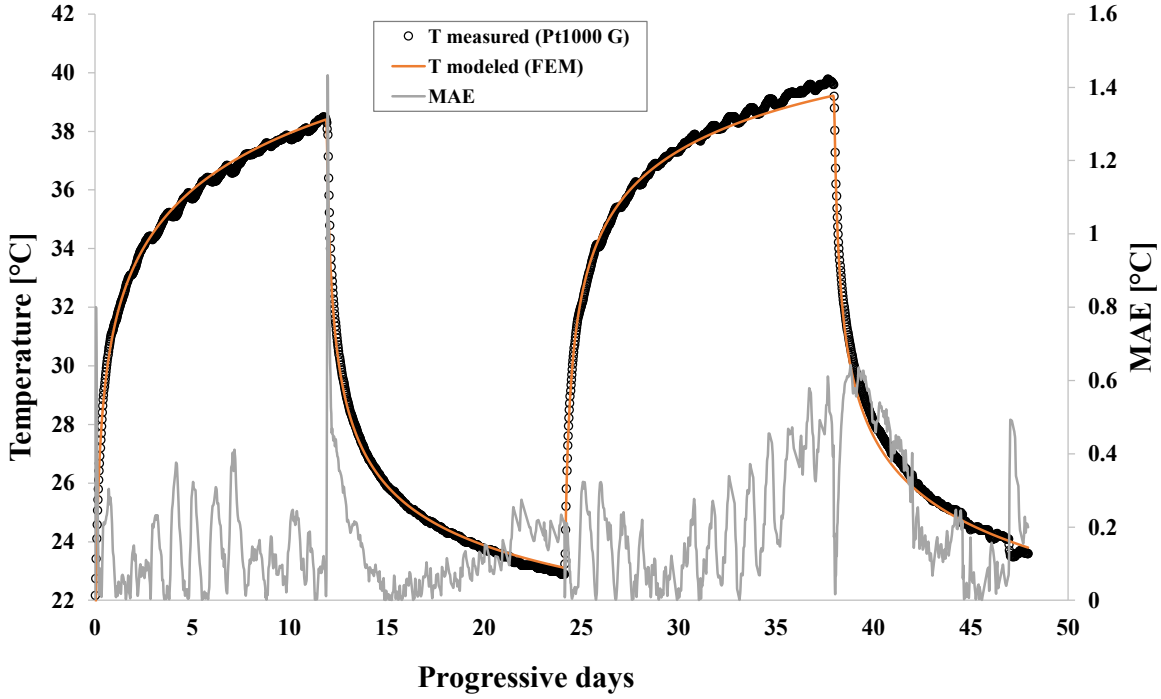

Figure 15. Comparison of temperature changes measured by Pt1000 G and that obtained from FEM simulations for TRTs no. 2 and 3.

The results of the experimental and the numerical analyses conducted through the use of both analytical solutions and FEM simulation models made it possible to characterize the thermophysical properties of soils as they change in depth. These values have been summarized in Table 4.

Table 4. Thermophysical parameters defined for the soil.

Pt1000	**z**	**λ_s**	**α_s**
[-]	[m]	[W/(m·K)]	[m^2/s]
C	1.27	1.17	$5.0 \cdot 10^{-7}$
D	2.27	1.97	$5.2 \cdot 10^{-7}$
E	4.27	1.52	$5.8 \cdot 10^{-7}$
F	7.27	1.63	$9.2 \cdot 10^{-7}$
G	13.27	1.74	$7.5 \cdot 10^{-7}$
I	23.27	1.82	$6.7 \cdot 10^{-7}$

Finally, from data in Table 4, through a weighted average over the thicknesses, it was possible to define the following average values of soil properties that were used as input into the TRNSYS model: $\lambda_s = 1.68$ W/(m·K) and $\alpha_s = 7.16 \cdot 10^{-7}$ m^2/s.

It is worth noting that averaging the thermal diffusivity values up to a depth of about 7 m yields an average value of about $\alpha_s = 7.10 \cdot 10^{-7}$ m^2/s, which differs, in terms of relative percent error, only by 5.6 % from the value obtained by the previously described methodology based on Eq. (2). This result confirms the ability of the proposed method to be used for thermophysical characterization of heterogeneous soil layers. Moreover, unlike what has been shown in the literature [24], this characterization can be conducted through the use of TRT results, although performed in an unconventional way, at a stage prior to construction.

3.1.2 Characterization of the road thermal collector thermophysical soil properties

Experimental data measured on the RTC prototype and FEM simulations, using the one-dimensional models, enabled the thermophysical characterization of the collector stratigraphy. The data obtained from the simulations have been summarized in Table 5.

Table 5. Thermophysical parameter of the RTC layers.

Layer	**Thickness**	**λ**	**α**
[-]	[kg/m^3]	[W/(m·K)]	[m^2/s]
Asphalt-binder	2000	0.89	$5.0 \cdot 10^{-7}$
Conductive concrete	2250	1.83	$8.5 \cdot 10^{-7}$
Lightweight concrete	1813	0.95	$5.5 \cdot 10^{-7}$
Soil	1804	1.17	$5.0 \cdot 10^{-7}$

As an example, a comparison between the temperature measured by the Pt100 C installed in the prototype RTC and that calculated through FEM simulations are shown in Fig. 16. In this figure, the results obtained in terms of MAE using Eq. (11) are reported, which reach a maximum value of 1.96 °C and a total value of 0.28 °C. The MAPE was also calculated on the same dataset using Eq. (12), and a percentage error of 1.7% was obtained.

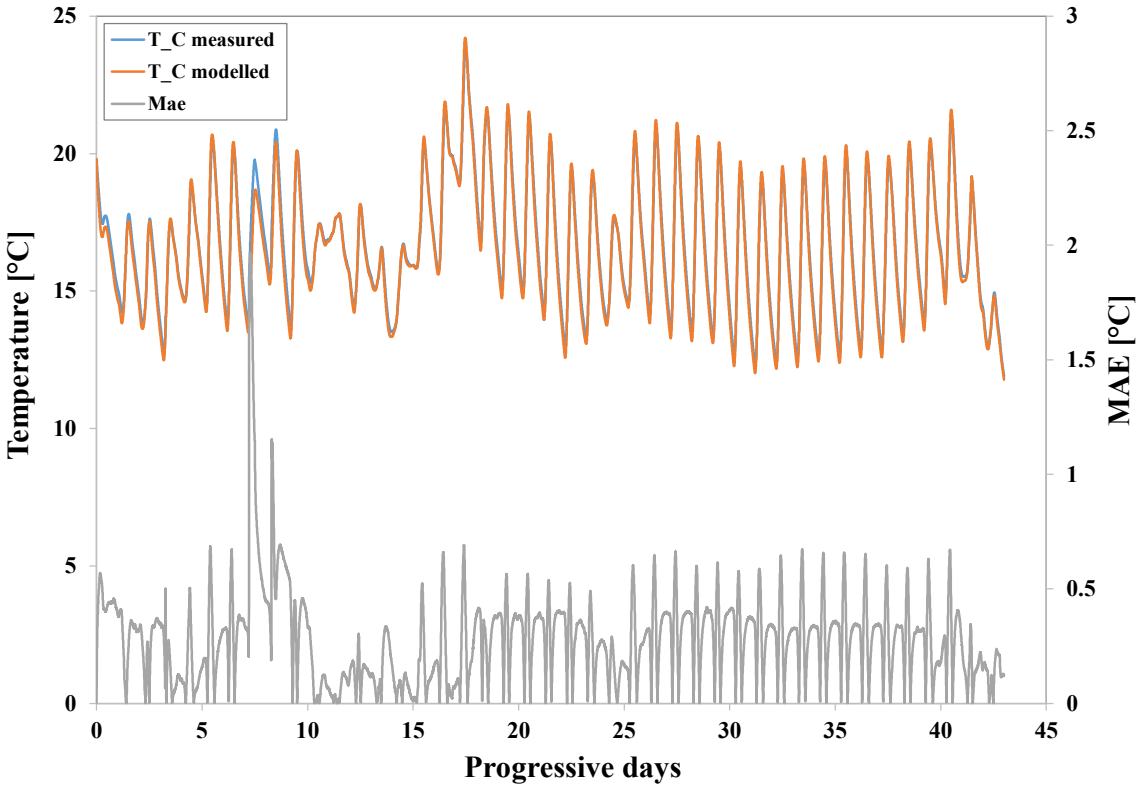

Figure 16. Comparison between the temperature measured by the Pt100 C and results from FEM simulations.

It is interesting to note here, too, that the methodology proposed in this paper to characterize the materials of the RTC is significantly more efficient than what has been proposed recently in the literature [33] in that, at the preliminary stage of collector construction, it is possible to determine the thermal diffusivity of all materials, as well as their conductivity, excluding the possible disturbance effect due to possible variations in the flow rates of the water flowing in the exchanger tubes.

3.2 Results from numerical simulation of the plant

After calibrating the TRNSYS model with the parameters obtained from the characterization of the soils and materials of the RTC, a series of parameter simulations of the operation of the plant during the first 5 years of its life were carried out. These simulations were conducted by varying the temperature range between the inlet and outlet from the dry-cooler to find the value that minimizes the annual changes in the internal energy of the volume of soil in which the BHEs are

made. The thermal jump value obtained for the system under study is about 4°C. The results presented below refer to this case.

Table 6 summarizes the monthly thermal energy productions and corresponding solar-to-thermal conversion efficiencies of the RTC calculated through simulations for the fourth year of the BTES charging period. The efficiency of the RTC was calculated from the monthly solar irradiation values and considering the collecting surface of the RTC (100 m^2). These data show a seasonal thermal energy production of 13.5 MWh corresponding to an average RTC efficiency of about 10%. The most productive month is July with an average monthly efficiency of 13 %. Hourly-based simulation results show that the RTC is characterized by an average seasonal heat power output of approximately 5.16 kW and a peak of 13.60 kW.

Table 6. Monthly energy productions and solar-to-thermal efficiency of the RTC

Month	**Solar irradiation**	**Thermal energy produced**	**RTC efficiency**
[-]	[kWh/m^2]	[kWh]	[%]
April	169	1392	8.3
May	218	2342	10.8
June	229	2828	12.4
July	244	3245	13.3
August	209	2450	11.7
September	154	1053	6.8
October	118	176	1.5
	100598	**13485**	**10.1**

As can be observed in Figure 17, during the subsequent winter period, about 79% of the energy transferred from the RTC to the BTES is recovered (10.60 MWh) and delivered to the dry-cooler. Over the first four years of operation, the average storage efficiency can be estimated at around 75% (a value consistent with data from previous analogous studies [11]).

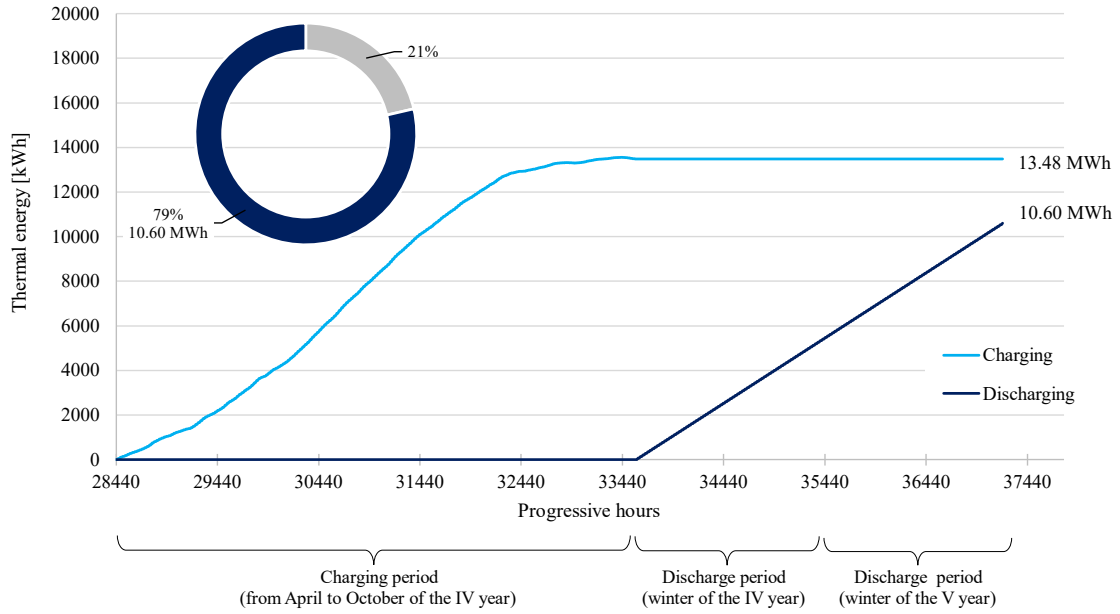

Figure 17. Cumulative energies related to the charging and discharging phase of the BTES during the winter between the year IV and V

Figure 18 shows the evolution of BTES inlet and outlet temperatures ($T_{i,\ BTES}$ and $T_{o,\ BTES}$, respectively) along with the average BTES soil temperature $T_{s,BTES}$ over the first five years of plant operations. The results depicted in Figure 18 show the typical long-term temperature trend of a BTES in which, over the years, the soil regions surrounding the BTES volume get warmer and warmer with a gradual reduction of thermal losses from the storage [7].

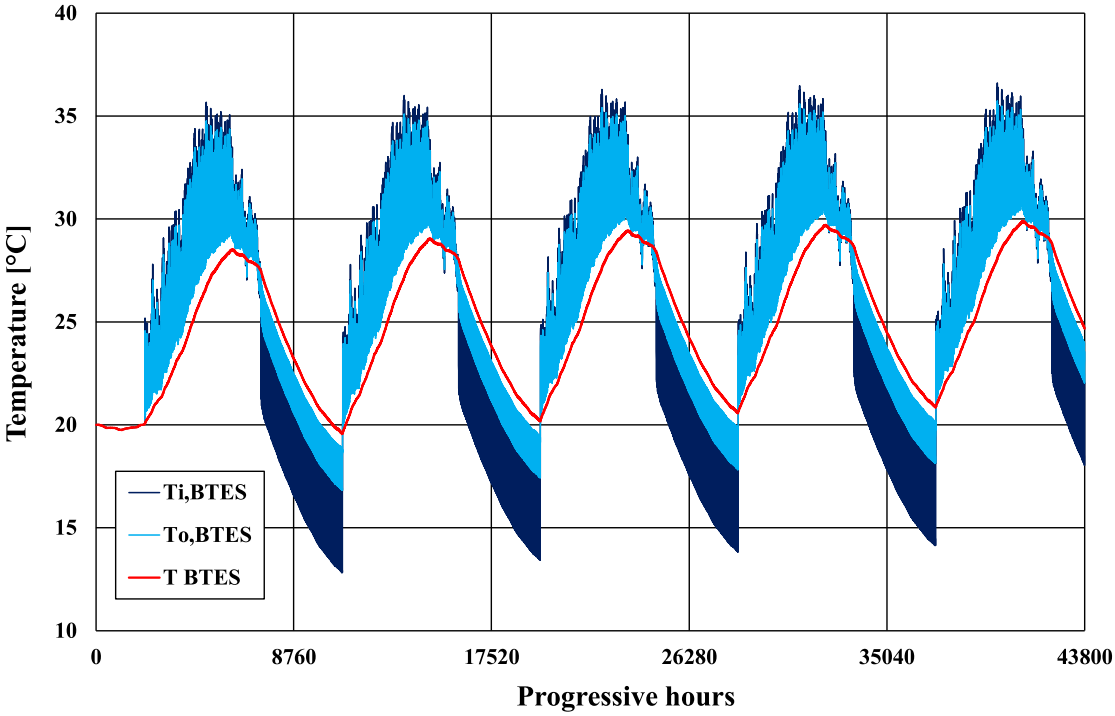

Figure 18. Variations of $T_{i,BTES}$, $T_{o,BTES}$ and $T_{s,BTES}$ in the first 5 years of plant operation.

Analyzing the typical annual values of these temperatures, e.g. considering the fourth year of operation, it is possible to observe: an average temperature of the water circulating in the RTC-BTES circuit during the charging period of about 30 °C (with a peak temperature of the water entering the BTES of $T_{i,BTES}$ = 36 °C) and an increase of the $T_{s,BTES}$ of about 8 °C. In the subsequent BTES discharge period, the temperature of the water supplied to the user reduced from $T_{o,BTES}$ = 27.76 °C (at the beginning of November) to $T_{o,BTES}$ = 18.13 °C (at the end of March) with an average value, over the winter period, of approximately 21.69 °C. In the same period, the average temperature of the air is equal to T_{air} = 14.94 °C.

To achieve the same water temperature value at the outlet of the BTES (21.69°C), a conventional GHP would require a total probe length 3.3 times longer than the one used in the analyzed BTES system in this study. Specifically, assuming a number of 8 header pipes spaced 8 m apart, each probe would need to reach a depth of 155 m to achieve the desired average outlet temperature.

The results of both the *in situ* experimental campaigns that are planned to be carried out on both the RTC and the BTES and the long-term monitoring of the pilot plant will allow the validation of the preliminary results obtained in this work.

Please cite this paper as: ***Buscemi, A., Beccali, M., Guarino, S., & Lo Brano, V. (2023). Coupling a road solar thermal collector and borehole thermal energy storage for building heating: First experimental and numerical results. Energy Conversion and Management, 291, 117279.***

Conclusions

The present study explored the possibility of integrating a RTC and a BTES storage to develop a sustainable heating system for a building located in a Mediterranean area. A pilot plant was set up at the test site of the University of Palermo, comprising an RTC with a surface area of 100 m^2 and a BTES consisting of 24 borehole heat exchangers (BHEs) with a depth of 15 m, constructed in a volume of soil of about 2000 m^3.

A novel methodology for the complete characterization of the thermophysical properties of the soils and materials constituting the RTC and BTES was developed. The methodology involved the construction of a pilot BHE and a pilot RTC, both instrumented with temperature sensors, and the execution of non-conventional TRTs using heating cables. The interpretation of the experimental data was performed using back analysis techniques based on analytical and numerical models, allowing the characterization of the thermal conductivity and diffusivity of the different soil layers and materials constituting the RTC. The average values of these properties for the subsurface of the Palermo area were estimated to be $\alpha_s = 7.16 \cdot 10^{-7}$ m^2/s and $\lambda_s = 1.68$ W/m^{-1} K^{-1}. For the determination of the thermal properties of the materials constituting the RTC, general relationships were implemented in the numerical models, relating thermal conductivity to density, reducing the number of parameters to be estimated. A TRNSYS numerical model of the pilot plant was developed and calibrated with the parameters obtained from the experimental campaign. The results of the simulations showed that the RTC had a peak power of approximately 13.60 kW and was capable of producing around 13.5 MWh of thermal energy annually during the summer period, at an average temperature of 30°C. Around 79% of the thermal energy produced by the RTC could be recovered from the BTES (10.6 MWh) during the winter period and supplied to the user at an average temperature of 22°C, demonstrating the validity of the proposed system.

Additional numerical analyses showed that a conventional GHP system constructed on the same soil should have a total linear development of BHEs at least three times that of the RTC-BTES system to provide the same energy during the winter period with the same average annual temperature values as the pilot system. Long-term monitoring of the plant during the years of operation will allow verification of the preliminary results presented in this study.

Please cite this paper as: ***Buscemi, A., Beccali, M., Guarino, S., & Lo Brano, V. (2023). Coupling a road solar thermal collector and borehole thermal energy storage for building heating: First experimental and numerical results. Energy Conversion and Management, 291, 117279.***

Acknowledgements

This work received funding from the project SmartEP (CUP: G58I18000770007) financed within the call POFESR Sicilia 2014–2020 Azione 1.1.5 "Sostegno all'avanzamento tecnologico delle imprese attraverso il finanziamento di linee pilota e azioni di validazione precoce dei prodotti e di dimostrazione su larga scala".

Nomenclature

a	short-wave radiation absorptivity, [-]
A_{sup}	amplitude in Eq. (2), [K]
c_p	specific heat, [J·kg^{-1}·K^{-1}]
B	constant in the Eq. (13), [-]
C	heat capacity, [J·m^{-3}·K^{-1}]
d	distance, [m]
D	diameter, [m]
G_h	global solar irradiance on a horizontal surface, [W·m^{-2}]
h	convective heat transfer coefficient, [W·m^{-2}·K^{-1}]
H	depth, [m]
k	constant in Eq. 4, [K]
m_w	constant in Eq. 4, [K]
$\dot{m}_w$	mass flow rate, [kg·s^{-1}]
n	porosity of the soil, [-]
N	number, [-]
q	heat injection rate per meter of borehole length, [W·m^{-1}]
R	thermal resistance, [K·m·W^{-1}]
Re	Reynold's number, [-]
t	time variable [s]
t_0	time-lag in Eq. (2), [s]
T	temperature, [K]
$\overline{T}$	average value of the temperature, [K]
$\overline{T}_w$	average value of the water temperature, [K]

Please cite this paper as: ***Buscemi, A., Beccali, M., Guarino, S., & Lo Brano, V. (2023). Coupling a road solar thermal collector and borehole thermal energy storage for building heating: First experimental and numerical results. Energy Conversion and Management, 291, 117279.***

T_{air} air temperature, [K]

T_{sup} surface temperature in Eq. (2), [K]

T_{sky} apparent temperature of the sky, [K]

v_{wind} wind velocity, [m·s-1]

V volume, [m^3]

x radius from the center of the borehole, [m]

z spatial coordinate, [m]

Greek letters

α thermal diffusivity, [m^2/s]

ε long-wave radiation emissivity, [-]

λ thermal conductivity, [W/(m·K)]

ρ density, [kg/m^3]

σ Stefan–Boltzmann constant 5.67×10−8 [W m−2 K−4]

τ period in Eq. (2), [s]

ω pulse in Eq. (2), [1/s]

Subscripts

a asphalt

b borehole

c concrete

g grout

i inner

o outer

p pipe

TS thermal sensor

Acronyms

Please cite this paper as: ***Buscemi, A., Beccali, M., Guarino, S., & Lo Brano, V. (2023). Coupling a road solar thermal collector and borehole thermal energy storage for building heating: First experimental and numerical results. Energy Conversion and Management, 291, 117279.***

BHE	Borehole Heat Exchanger
BTES	Borehole Thermal Energy Storage
CHP	Combined Heat and Power systems
DST	Duct Ground Heat Storage Model
EPS	Expanded Polystyrene
EU	European Union
FEM	Finite Element Method
GHP	Geothermal Heat Pumps
HTF	Heat Transfer Fluid
HVAC	Heating Ventilating and Air Conditioning
MAE	Mean Absolute Error
MAPE	Mean Absolute Percentage Error
PDE	Partial Differential Equation
PeX-A	Abbreviation for cross-linked, high-density polyethylene material
RTC	Road Thermal Collector
SMARTEP	Sustainable Model and Renewable Thinking Energy Parking
STES	Seasonal Thermal Energy Storage systems
TMY	Typical Meteorological Year
TRNSYS	Transient System Simulation Tool
TRT	Thermal Response Test

References

[1] (IEA) IEA. https://www.iea.org/data-and-statistics 2019.

[2] Ürge-Vorsatz D, Cabeza LF, Serrano S, Barreneche C, Petrichenko K. Heating and cooling energy trends and drivers in buildings. Renew Sustain Energy Rev 2015;41. https://doi.org/10.1016/j.rser.2014.08.039.

[3] Mahon H, O'Connor D, Friedrich D, Hughes B. A review of thermal energy storage technologies for seasonal loops. Energy 2022;239. https://doi.org/10.1016/j.energy.2021.122207.

[4] Lanahan M, Tabares-Velasco PC. Seasonal thermal-energy storage: A critical review on BTES systems, modeling, and system design for higher system efficiency. Energies

2017;10. https://doi.org/10.3390/en10060743.

[5] Welsch B, Göllner-Völker L, Schulte DO, Bär K, Sass I, Schebek L. Environmental and economic assessment of borehole thermal energy storage in district heating systems. Appl Energy 2018;216. https://doi.org/10.1016/j.apenergy.2018.02.011.

[6] Ushamah HM, Ahmed N, Elfeky KE, Mahmood M, Qaisrani MA, Waqas A, et al. Techno-economic analysis of a hybrid district heating with borehole thermal storage for various solar collectors and climate zones in Pakistan. Renew Energy 2022;199:1639–56. https://doi.org/10.1016/J.RENENE.2022.09.059.

[7] Guo F, Zhu X, Zhang J, Yang X. Large-scale living laboratory of seasonal borehole thermal energy storage system for urban district heating. Appl Energy 2020;264. https://doi.org/10.1016/j.apenergy.2020.114763.

[8] Kizilkan O, Dincer I. Borehole thermal energy storage system for heating applications: Thermodynamic performance assessment. Energy Convers Manag 2015;90. https://doi.org/10.1016/j.enconman.2014.10.043.

[9] Durga S, Beckers KF, Taam M, Horowitz F, Cathles LM, Tester JW. Techno-economic analysis of decarbonizing building heating in Upstate New York using seasonal borehole thermal energy storage. Energy Build 2021;241. https://doi.org/10.1016/j.enbuild.2021.110890.

[10] Pokhrel S, Amiri L, Poncet S, Sasmito AP, Ghoreishi-Madiseh SA. Renewable heating solutions for buildings; a techno-economic comparative study of sewage heat recovery and Solar Borehole Thermal Energy Storage System. Energy Build 2022;259. https://doi.org/10.1016/j.enbuild.2022.111892.

[11] Panno D, Buscemi A, Beccali M, Chiaruzzi C, Cipriani G, Ciulla G, et al. A solar assisted seasonal borehole thermal energy system for a non-residential building in the Mediterranean area. Sol Energy 2019;192. https://doi.org/10.1016/j.solener.2018.06.014.

[12] Maragna C, Rey C, Perreaux M. A novel and versatile solar Borehole Thermal Energy Storage assisted by a Heat Pump. Part 1: System description. Renew Energy 2023;208:709–25. https://doi.org/10.1016/J.RENENE.2023.03.105.

[13] Guo F, Zhu X, Li P, Yang X. Low-grade industrial waste heat utilization in urban district heating: Simulation-based performance assessment of a seasonal thermal energy storage system. Energy 2022;239. https://doi.org/10.1016/j.energy.2021.122345.

[14] Cui Y, Zhang F, Shao Y, Twaha S, Tong H. Techno-Economic Comprehensive Review of State-of-the-Art Geothermal and Solar Roadway Energy Systems. Sustain 2022;14. https://doi.org/10.3390/su141710974.

[15] Bobes-Jesus V, Pascual-Muñoz P, Castro-Fresno D, Rodriguez-Hernandez J. Asphalt solar collectors: A literature review. Appl Energy 2013;102. https://doi.org/10.1016/j.apenergy.2012.08.050.

[16] Ghalandari T, Hasheminejad N, Van den bergh W, Vuye C. A critical review on large-scale research prototypes and actual projects of hydronic asphalt pavement systems. Renew Energy 2021;177. https://doi.org/10.1016/j.renene.2021.06.010.

[17] Jaiswal P, Anupam BR, Chandrappa AK, Sahoo UC. Harvesting heat energy using geothermal and hydronic pavements for sustainable cities: A comprehensive review of an emerging idea. Sustain Cities Soc 2023;93. https://doi.org/10.1016/j.scs.2023.104539.

[18] Xu L, Wang J, Xiao F, EI-Badawy S, Awed A. Potential strategies to mitigate the heat island impacts of highway pavement on megacities with considerations of energy uses. Appl Energy 2021;281. https://doi.org/10.1016/j.apenergy.2020.116077.

[19] Wołoszyn J, Gołaś A. Sensitivity analysis of efficiency thermal energy storage on selected rock mass and grout parameters using design of experiment method. Energy Convers Manag 2014;87. https://doi.org/10.1016/j.enconman.2014.03.059.

[20] Welsch B, Rühaak W, Schulte DO, Bär K, Sass I. Characteristics of medium deep borehole thermal energy storage. Int J Energy Res 2016;40. https://doi.org/10.1002/er.3570.

[21] Wołoszyn J. Global sensitivity analysis of borehole thermal energy storage efficiency on the heat exchanger arrangement. Energy Convers Manag 2018;166. https://doi.org/10.1016/j.enconman.2018.04.009.

[22] Wołoszyn J. Global sensitivity analysis of borehole thermal energy storage efficiency for seventeen material, design and operating parameters. Renew Energy 2020;157. https://doi.org/10.1016/j.renene.2020.05.047.

[23] Brown CS, Kolo I, Falcone G, Banks D. Repurposing a deep geothermal exploration well for borehole thermal energy storage: Implications from statistical modelling and sensitivity analysis. Appl Therm Eng 2023;220:119701. https://doi.org/10.1016/J.APPLTHERMALENG.2022.119701.

[24] Li P, Guo F, Yang X. An inversion method to estimate the thermal properties of

heterogeneous soil for a large-scale borehole thermal energy storage system. Energy Build 2022;263. https://doi.org/10.1016/j.enbuild.2022.112045.

[25] Nilsson E, Rohdin P. Performance evaluation of an industrial borehole thermal energy storage (BTES) project – Experiences from the first seven years of operation. Renew Energy 2019;143. https://doi.org/10.1016/j.renene.2019.05.020.

[26] Nilsson E, Rohdin P. Empirical validation and numerical predictions of an industrial borehole thermal energy storage system. Energies 2019;12. https://doi.org/10.3390/en12122263.

[27] Xu L, Guo F, Hoes PJ, Yang X, Hensen JLM. Investigating energy performance of large-scale seasonal storage in the district heating system of chifeng city: Measurements and model-based analysis of operation strategies. Energy Build 2021;247. https://doi.org/10.1016/j.enbuild.2021.111113.

[28] Hellström G. Ground heat storage: Thermal analyses of duct storage systems. Lund Univ 1991.

[29] Johnsson J, Adl-Zarrabi B. A numerical and experimental study of a pavement solar collector for the northern hemisphere. Appl Energy 2020;260. https://doi.org/10.1016/j.apenergy.2019.114286.

[30] Ghalandari T, Ceulemans D, Hasheminejad N, Guldentops G, Van den bergh W, Verhaert I, et al. A simplified model to assess the thermal performance of pavement solar collectors. Appl Therm Eng 2021;197. https://doi.org/10.1016/j.applthermaleng.2021.117400.

[31] Ghalandari T, Baetens R, Verhaert I, SNM Nasir D, Van den bergh W, Vuye C. Thermal performance of a controllable pavement solar collector prototype with configuration flexibility. Appl Energy 2022;313. https://doi.org/10.1016/j.apenergy.2022.118908.

[32] Motamedi Y, Makasis N, Gu X, Narsilio GA, Arulrajah A, Horpibulsuk S. Numerical investigation of geothermal pavements: Design optimisation & boundary conditions. Transp Geotech 2022;37. https://doi.org/10.1016/j.trgeo.2022.100843.

[33] Songok J, Mäkiranta A, Rapantova N, Pospisil P, Martinkauppi B. Numerical simulation of heat recovery from asphalt pavement in Finnish climate conditions. Int J Therm Sci 2023;187. https://doi.org/10.1016/j.ijthermalsci.2023.108181.

[34] Buscemi A, Catrini P, Piacentino A, Cardona F. Energy-saving potential of ground source multiple chillers in simple and hybrid configurations for Mediterranean climates. Energy

Convers Manag 2022;263:115721. https://doi.org/10.1016/j.enconman.2022.115721.

[35] D'amico A, Ciulla G, Buscemi A, Panno D, Zinzi M, Beccali M. Road Thermal Collector for Building Heating in South Europe: Numerical Modeling and Design of an Experimental Set-Up. Energies 2022;15. https://doi.org/10.3390/en15020430.

[36] Schwarz H, Badenes B, Wagner J, Cuevas JM, Urchueguía J, Bertermann D. A case study of thermal evolution in the vicinity of geothermal probes following a distributed trt method. Energies 2021;14. https://doi.org/10.3390/en14092632.

[37] Hassn A, Chiarelli A, Dawson A, Garcia A. Thermal properties of asphalt pavements under dry and wet conditions. Mater Des 2016;91. https://doi.org/10.1016/j.matdes.2015.11.116.

[38] Asadi I, Shafigh P, Abu Hassan ZF Bin, Mahyuddin NB. Thermal conductivity of concrete – A review. J Build Eng 2018;20. https://doi.org/10.1016/j.jobe.2018.07.002.

[39] Carslow HS, Jaeger JC, Morral JE. Conduction of Heat in Solids, Second Edition. J Eng Mater Technol 1986;108. https://doi.org/10.1115/1.3225900.

[40] Florides GA, Pouloupatis PD, Kalogirou S, Messaritis V, Panayides I, Zomeni Z, et al. The geothermal characteristics of the ground and the potential of using ground coupled heat pumps in Cyprus. Energy 2011;36. https://doi.org/10.1016/j.energy.2011.05.048.

[41] Incropera FP, DeWitt DP, Bergman TL, Lavine AS. Fundamentals of Heat and Mass Transfer 5th Edition with IHT2.0/FEHT with Users Guides. Wiley; 2001.

[42] Signorelli S, Bassetti S, Pahud D, Kohl T. Numerical evaluation of thermal response tests. Geothermics 2007;36. https://doi.org/10.1016/j.geothermics.2006.10.006.

[43] Eskilson P. Thermal analysis of heat extraction boreholes 1987.

[44] No Title n.d.:http://www.comsol.com.

[45] Colangelo F, Roviello G, Ricciotti L, Ferrándiz-Mas V, Messina F, Ferone C, et al. Mechanical and thermal properties of lightweight geopolymer composites. Cem Concr Compos 2018;86. https://doi.org/10.1016/j.cemconcomp.2017.11.016.

[46] Honorio T, Bary B, Benboudjema F. Thermal properties of cement-based materials: Multiscale estimations at early-age. Cem Concr Compos 2018;87. https://doi.org/10.1016/j.cemconcomp.2018.01.003.

[47] Farlow SJ. Partial differential equations for scientists and engineers. Courier Corporation; 1993.

[48] Willmott CJ, Matsuura K. Advantages of the mean absolute error (MAE) over the root mean square error (RMSE) in assessing average model performance. Clim Res 2005;30:79–82.

[49] Hyndman RJ, Koehler AB. Another look at measures of forecast accuracy. Int J Forecast 2006;22:679–88.

[50] Klein SA. TRNSYS 17: A Transient System Simulation Program. Sol Energy Lab Univ Wisconsin, Madison, USA 2010;1.

[51] Hermansson Å. Mathematical model for calculation of pavement temperatures: Comparison of calculated and measured temperatures. Transp. Res. Rec., 2001. https://doi.org/10.3141/1764-19.

[52] Palyvos JA. A survey of wind convection coefficient correlations for building envelope energy systems' modeling. Appl Therm Eng 2008;28. https://doi.org/10.1016/j.applthermaleng.2007.12.005.

[53] Conti P, Testi D, Grassi W. Revised heat transfer modeling of double-U vertical ground-coupled heat exchangers. Appl Therm Eng 2016;106. https://doi.org/10.1016/j.applthermaleng.2016.06.097.

[54] Gnielinski V. On heat transfer in tubes. Int J Heat Mass Transf 2013;63. https://doi.org/10.1016/j.ijheatmasstransfer.2013.04.015.

[55] Sakellariou EI, Wright AJ, Axaopoulos P, Oyinlola MA. PVT based solar assisted ground source heat pump system: Modelling approach and sensitivity analyses. Sol Energy 2019;193:37–50. https://doi.org/10.1016/j.solener.2019.09.044.

[56] Meteonorm. Meteonorm - Global meteorological database. Meteotest 2012.